

High Dimensional Ensemble Kalman Filter

Shouxia Wang

School of Statistics and Management, Shanghai University of Finance and Economics

Hao-Xuan Sun

Center for Big Data Research, Peking University

and

Song Xi Chen*

Department of Statistics and Data Science, Tsinghua University

Abstract

The Ensemble Kalman Filter (EnKF), as a fundamental data assimilation approach, has been widely used in many fields of the sciences and engineering. When the state variable is of high dimensional accompanied with high resolution observations of physical models, some key theoretical aspects of the EnKF are open for investigation. This paper proposes several high dimensional EnKF (HD-EnKF) methods equipped with consistent estimators for the important forecast error covariance and Kalman Gain matrices. It then studies the theoretical properties of the EnKF under both fixed and high dimensional state variables, which provides one-step and multiple-step mean square errors of the analysis states to the underlying oracle states offered by the Kalman Filter and gives the much needed insight to the roles played by the forecast error covariance on the accuracy of the EnKF. The accuracy of the data assimilation under the misspecified physical model is also considered. Numerical studies on the Lorenz-96 and the Shallow Water Equation models illustrate that the proposed HD-EnKF algorithms outperform the standard EnKF and widely used inflation methods.

Keywords: Data Assimilation; Dynamic System; Ensemble Kalman Filter; High Dimensional Imputation.

*

1 Introduction

Kalman Filter (Kalman, 1960) is a fundamental approach for forecasting and data assimilation for a partially observed dynamic system. Data assimilation is a statistical procedure that combines information from numerical physical model forecasts with observed data to obtain the best possible description of a dynamical system and its uncertainty (Evensen et al., 2022). The assimilated state variables at a time are used to generate the forecast for the next time step. For chaotic systems sensitive to initial values, data assimilation can significantly improve the accuracy of the forecast by using optimized state variables as initial values (Lorenz, 1963). Although much applied in numerical weather and oceanography prediction, Kalman Filter and its later developments (EnKF, three and four-dimensional variational assimilation (3D-Var, 4D-Var; Pailleux, 1990; Courtier et al., 1998)) are the methodological core for scientific algorithms over various fields, including hydrology, remote sensing data inversion, carbon data assimilation, robotic control and automatic driving. Data assimilation methods also provide the underlying algorithms and predictive techniques for building digital twins for social and economic systems.

The limitations of the Kalman Filter are (i) it assumes a linear model which is restrictive for many non-linear dynamic systems; and (ii) the forecast error covariance and Kalman Gain matrices are expensive to store and update when the dimension of the state vector is large. To overcome these limitations, Evensen (1994) proposed the Ensemble Kalman Filter (EnKF), where the forecast error covariance is estimated by the sample covariance based on generated forecast ensembles. The EnKF only requires storing and operating on much reduced-size state vectors and the ensembles can be generated in parallel. These advantages have made the EnKF an effective and widely used data assimilation scheme.

Estimating the forecast error covariance is a key in the EnKF, which is made in the

EnKF by the sample covariance of the forecast ensembles. Past works on the EnKF found that the sampling error can lead to underestimation of the forecast error covariance and can eventually cause filter divergence (Anderson and Anderson, 1999; Constantinescu et al., 2007). Filter divergence refers to a decreasing ability to correct the ensemble state towards the observations after certain rounds of assimilation. One reason for the filter divergence is the variance of the ensemble forecast error becomes too small when there are unaccounted model errors (Lorenz, 2003); the other is due to the substantial mismatch between the estimated and true error covariance matrices (Houtekamer and Mitchell, 1998; Constantinescu et al., 2007).

Along with advances in remote sensing technology in measuring the Earth system, there is a growing availability of high spatio-temporal resolution satellite observations (Stroud et al., 2010; Guinehut et al., 2012; Lellouche et al., 2013). Meanwhile, the high resolution dataset and forecasting are in increasing demands in modern meteorology and atmospheric systems like high resolution weather forecasting, global carbon calculation and ocean data assimilation, which leads to high dimensional geophysical models with high dimensional state vectors. The high dimensional state vectors lead to high dimensional forecast error covariance and Kalman Gain matrices. The high dimensionality is known to cause the non-convergence of the sample forecast error covariance (Bai and Yin, 1993), felt in the form of filter divergence and unreliable data assimilation in practice. Geophysicists have proposed two methods to counter the problems, the localization method (Furrer et al., 2006; Furrer and Bengtsson, 2007) that sets covariances to zero for the geographical distances bigger than a threshold and the inflation method that enlarges the forecast error covariance by adding either a multiplicative factor or an additive term (Wang and Bishop, 2003; Constantinescu et al., 2007; Liang et al., 2012). However, the statistical properties of these methods are

yet to be established. [Tong \(2018\)](#) investigated the performance of the local EnKF with domain localization under linear systems. [Katzfuss et al. \(2020\)](#) proposed Gibbs EnKF and particle EnKF algorithms for high dimensional hierarchical dynamic models from a Bayesian perspective. [Al-Ghattas and Sanz-Alonso \(2024\)](#) developed a non-asymptotic analysis on the difference between the ensembles of single-step Ensemble Kalman Inversion using the true and the localized estimation of forecast error covariances under the framework of effective dimension of matrices and [Al-Ghattas et al. \(2024\)](#) explored the resampling EnKF under linear systems and effective dimension. While [Al-Ghattas et al. \(2025\)](#) studied the difference between the ensembles of single-step EnKF using the true and the thresholded estimation of forecast error covariance functions in a small correlation lengthscale regime. The EnKF methods and their theoretical analysis under high dimensional framework for general non-linear models, especially the theoretical performance of the multiple-step EnKF under both the correct and misspecified models, need further investigation.

This paper proposes several high dimensional EnKF (HD-EnKF) methods and conducts a theoretical analysis of the one-step and multiple-step assimilated state vectors for general nonlinear models and imperfect models under both fixed and high dimensional cases. It is shown that even at the high dimensional setting, the mean square errors (MSEs) of the analysis states by the EnKF could be controlled by the error bounds of the high dimensional forecast error covariance estimators. Thus, consistent recovery of the underlying analysis states can be attained by the proposed HD-EnKF. Specifically, we establish the MSE bounds and weak convergence of the analysis states from the HD-EnKF to the underlying analysis under both fixed and high dimensional cases, as well as for both correct and imperfect physical models. The MSE bounds for the multiple-step forecast and assimilation are also provided. The investigation of the HD-EnKF under the misspecified model gives a

more realistic description of the performance of the EnKF. Under the misspecified model, the MSE not only depends on the estimation error of the forecast error covariance matrices but also the discrepancy between the misspecified and the true model. Simulation studies suggest that the proposed HD-EnKF could achieve more accurate and robust assimilation results than the widely used inflation-based EnKF method. This implies that the proposed HD-EnKF is applicable in a range of studies and prospects in earth science like global carbon calculation, weather forecasting and the production of high resolution data sets, considering both the theoretical guarantee and better performances in practice.

The paper is structured as follows. Section 2 reviews the Kalman Filter and the EnKF. Section 3 presents several consistent estimators of the high dimensional forecast error covariance and the key Kalman Gain, and establishes the theoretical properties of the EnKF. The effects of imperfect or misspecified models on the accuracy of the EnKF are provided in Section 4. Results of empirical data assimilation based on two well-known geophysical models are reported in Section 5, followed by a conclusion in Section 6. The proposed HD-EnKF algorithms, additional theoretical and simulation results, and technical details are given in the Supplementary Material (SM).

2 Review on Kalman and Ensemble Kalman Filters

The Kalman Filter (Kalman, 1960) assumes the following linear Gaussian state-space model (which was generalized to nonlinear models in the EnKF)

$$\begin{cases} \mathbf{x}_t = \mathbf{M}_t \mathbf{x}_{t-1} + \mathbf{w}_t, & \mathbf{w}_t \sim N_p(\mathbf{0}, \mathbf{Q}_t), \\ \mathbf{y}_t = \mathbf{H}_t \mathbf{x}_t + \boldsymbol{\varepsilon}_t, & \boldsymbol{\varepsilon}_t \sim N_q(\mathbf{0}, \mathbf{R}_t), \end{cases} \quad (2.1)$$

where \mathbf{x}_t is the p -dimensional not fully observed state vector of a dynamic system at time t , \mathbf{M}_t is the linear model operator (also called evolution or forecast operator), \mathbf{w}_t is the

model error term with \mathbf{Q}_t as its covariance, \mathbf{y}_t is the q -dimensional observation vector at time t , \mathbf{H}_t is a linear observation operator which relates the state \mathbf{x}_t to the observation \mathbf{y}_t , and $\boldsymbol{\varepsilon}_t$ is the observation error with \mathbf{R}_t being its covariance matrix.

Assuming \mathbf{M}_t , \mathbf{Q}_t , \mathbf{H}_t , and \mathbf{R}_t are known, the Kalman Filter provides a two-step alternative updating framework based on the theory of multivariate normal distribution. In the forecast step, suppose that $\mathbf{x}_{t-1} \mid \mathbf{y}_{1:t-1} \sim \mathcal{N}_p(\mathbf{x}_{t-1}^a, \Sigma_{t-1}^a)$, where \mathbf{x}_{t-1}^a is the analysis state vector at the previous time $t-1$ and $\mathbf{y}_{1:t-1}$ denotes the observation $\{\mathbf{y}_i\}_{i=1}^{t-1}$ up to time $t-1$, the conditional distribution of \mathbf{x}_t given $\mathbf{y}_{1:t-1}$ is

$$\mathbf{x}_t \mid \mathbf{y}_{1:t-1} \sim \mathcal{N}_p(\mathbf{x}_t^f, \Sigma_t^f) \equiv \mathcal{N}_p(\mathbf{M}_t \mathbf{x}_{t-1}^a, \mathbf{M}_t \Sigma_{t-1}^a \mathbf{M}_t^T + \mathbf{Q}_t), \quad (2.2)$$

where $\mathbf{x}_t^f = \mathbf{M}_t \mathbf{x}_{t-1}^a$ is the forecast state and

$$\Sigma_t^f = \mathbf{M}_t \Sigma_{t-1}^a \mathbf{M}_t^T + \mathbf{Q}_t, \quad (2.3)$$

is the forecast error covariance, the variance of the forecast error $\mathbf{x}_t - \mathbf{x}_t^f$.

In the update (assimilation) step, the goal is to update \mathbf{x}_t^f according to the new observation \mathbf{y}_t and to reduce the difference between the true state \mathbf{x}_t and the forecast state \mathbf{x}_t^f . The joint distribution of $(\mathbf{x}_t, \mathbf{y}_t)$ given $\mathbf{y}_{1:t-1}$ is Gaussian, which implies that $\mathbf{x}_t \mid \mathbf{y}_{1:t} \sim \mathcal{N}_p(\mathbf{x}_t^a, \Sigma_t^a)$, where, by the conditional Gaussian distribution formulae,

$$\mathbf{x}_t^a = \mathbf{x}_t^f + \mathbf{K}_t (\mathbf{y}_t - \mathbf{H}_t \mathbf{x}_t^f), \quad \Sigma_t^a = (\mathbf{I}_p - \mathbf{K}_t \mathbf{H}_t) \Sigma_t^f \quad \text{and} \quad (2.4)$$

$$\mathbf{K}_t = \Sigma_t^f \mathbf{H}_t^T (\mathbf{H}_t \Sigma_t^f \mathbf{H}_t^T + \mathbf{R}_t)^{-1}, \quad (2.5)$$

which are, respectively, the analysis (assimilation) state and the associated analysis covariance matrix, and the Kalman Gain matrix. Note that the analysis state \mathbf{x}_t^a is the minimum variance unbiased estimator for the mean of \mathbf{x}_t under the linear state-space model (2.1).

However, models in earth science or engineering are often nonlinear so that $\mathbf{x}_t = \mathcal{M}_t(\mathbf{x}_{t-1}) + \mathbf{w}_t$ in (2.1), where \mathcal{M}_t is a nonlinear model operator that can invalidate the

forecast distribution in (2.2). Besides, for large dynamic systems, the dimension of the state vector \mathbf{x}_t can be large so that the forecast error covariance Σ_t^f is expensive to compute and store. To tackle these problems, [Evensen \(1994\)](#) proposed the EnKF, where the forecast error covariance is no longer updated as (2.3) but by the sample covariance of n forecast ensembles. It hence only needs to store and operate on n vectors of dimension p , and is convenient for parallel computing, and thus improves the computing efficiency and reduces the storage cost.

The EnKF assumes possibly nonlinear model system with a linear observation operator, with the first equation in (2.1) replaced by

$$\mathbf{x}_t = \mathcal{M}_t(\mathbf{x}_{t-1}) + \mathbf{w}_t, \quad (2.6)$$

where \mathcal{M}_t is the possibly nonlinear model operator.

A key feature of the EnKF is to generate an ensemble of perturbed forecast states $\{\mathbf{x}_{t,j}^f\}_{j=1}^n$ of size n from the conditional distribution of \mathbf{x}_t given $\mathbf{y}_{1:t-1}$, which are used to estimate the forecast error covariance matrix Σ_t^f . Given the analysis ensemble at the previous time step $\{\mathbf{x}_{t-1,j}^a\}_{j=1}^n$, the EnKF consists of the following three steps.

Step (i): Run the model forward in time to get the perturbed forecast state and their average:

$$\mathbf{x}_{t,j}^f = \mathcal{M}_t(\mathbf{x}_{t-1,j}^a) + \mathbf{w}_{t,j}, \quad \hat{\mathbf{x}}_t^f = \frac{1}{n} \sum_{j=1}^n \mathbf{x}_{t,j}^f, \quad \mathbf{w}_{t,j} \stackrel{IID}{\sim} \mathcal{N}_p(\mathbf{0}, \mathbf{Q}_t). \quad (2.7)$$

Step (ii): Estimate the forecast error covariance matrix Σ_t^f by the sample covariance matrix of the forecast ensemble, namely

$$\hat{\Sigma}_t^f = (n-1)^{-1} \sum_{j=1}^n (\mathbf{x}_{t,j}^f - \hat{\mathbf{x}}_t^f)(\mathbf{x}_{t,j}^f - \hat{\mathbf{x}}_t^f)^T \triangleq \mathbf{S}_t^f, \quad (2.8)$$

and obtain the Kalman Gain estimate $\hat{\mathbf{K}}_t = \hat{\Sigma}_t^f \mathbf{H}_t^T (\mathbf{H}_t \hat{\Sigma}_t^f \mathbf{H}_t^T + \mathbf{R}_t)^{-1}$.

Step (iii): Calculate the perturbed residuals $\mathbf{d}_{t,j} = \mathbf{y}_t + \boldsymbol{\varepsilon}_{t,j} - \mathbf{H}_t \mathbf{x}_{t,j}^f$ where $\{\boldsymbol{\varepsilon}_{t,j}\}_{j=1}^n \stackrel{IID}{\sim} \mathcal{N}(\mathbf{0}, \mathbf{R}_t)$, and let $\mathbf{d}_t = n^{-1} \sum_{j=1}^n \mathbf{d}_{t,j}$. Compute the perturbed analysis states and their average, the analysis state,

$$\begin{aligned} \mathbf{x}_{t,j}^a &= \mathbf{x}_{t,j}^f + \hat{\Sigma}_t^f \mathbf{H}_t^T (\mathbf{H}_t \hat{\Sigma}_t^f \mathbf{H}_t^T + \mathbf{R}_t)^{-1} \mathbf{d}_{t,j}, \\ \hat{\mathbf{x}}_t^a &= \frac{1}{n} \sum_{j=1}^n \mathbf{x}_{t,j}^a = \hat{\mathbf{x}}_t^f + \hat{\Sigma}_t^f \mathbf{H}_t^T (\mathbf{H}_t \hat{\Sigma}_t^f \mathbf{H}_t^T + \mathbf{R}_t)^{-1} \mathbf{d}_t, \end{aligned} \quad (2.9)$$

which will be used for the data assimilation at the next time step.

In practice, the algorithm is initialized at time $t = 0$ by drawing $\{\mathbf{x}_{0,j}^a\}_{j=1}^n$ independently from $\mathcal{N}_p(\mathbf{x}_0^a, \Sigma_0^a)$ where \mathbf{x}_0^a and Σ_0^a are either chosen based on the physical model or by pre-running the physical model for a period of time. Then, the ensemble is propagated forward through time, alternating between the forecast and the analysis steps, according to the three-step procedure above. If \mathbf{R}_t and \mathbf{Q}_t are unknown, their estimates can be entertained to substitute them in (2.7) and (2.9).

The EnKF does not require the expensive recursions (2.3) and (2.4)-(2.5) used in the Kalman Filter. Instead, it estimates the forecast error covariance Σ_t^f by the sample covariance. For the case with non-linear model operator as in (2.6), we can still define the underlying analysis state \mathbf{x}_t^a by (2.4)-(2.5), where $\mathbf{x}_t^f = \mathbb{E}(\mathbf{x}_t \mid \mathbf{y}_{1:t-1}) = \mathbb{E}(\mathcal{M}_t(\mathbf{x}_{t-1}) + \mathbf{w}_t \mid \mathbf{y}_{1:t-1})$ is the forecast state and Σ_t^f is the forecast error covariance $\Sigma_t^f = \text{var}((\mathbf{x}_t - \mathbf{x}_t^f) \mid \mathbf{y}_{1:t-1})$. In fact, $\hat{\mathbf{x}}_t^a$ defined by (2.9) is the solution to the minimizing problem (2.10)

$$J(\mathbf{x}) = \frac{1}{2} \{ (\mathbf{x} - \hat{\mathbf{x}}_t^f)^T (\hat{\Sigma}_t^f)^{-1} (\mathbf{x} - \hat{\mathbf{x}}_t^f) + (\mathbf{y}_t - \mathbf{H}_t \mathbf{x})^T \mathbf{R}_t^{-1} (\mathbf{y}_t - \mathbf{H}_t \mathbf{x}) \}, \quad (2.10)$$

and \mathbf{x}_t^a defined by (2.4)-(2.5) is the solution to the above minimizing problem with $\hat{\mathbf{x}}_t^f$ and $\hat{\Sigma}_t^f$ replaced by \mathbf{x}_t^f and Σ_t^f . For the ease of reference, and to avoid differentiating between the linear and the non-linear cases, we also call \mathbf{x}_t^a as the analysis state of the Kalman Filter even in the non-linear model case. The next two sections will establish the convergence of the EnKF analysis state $\hat{\mathbf{x}}_t^a$ to the underlying \mathbf{x}_t^a of the Kalman Filter.

3 Convergence of Ensemble Kalman Filter

We first provide the upper bound of the estimation error of the estimated Kalman Gain matrix. Throughout the paper, $\|\cdot\|$ denotes the L_2 (spectral) norm of a matrix or the L_2 norm of a vector, while other matrix norms will be specified explicitly. For two positive sequences a_n and b_n , $a_n \asymp b_n$, $a_n \ll b_n$ and $a_n \gg b_n$ mean that a_n/b_n is bounded away from zero and infinity, $a_n/b_n \rightarrow 0$ and $b_n/a_n \rightarrow 0$ as $n \rightarrow \infty$, respectively. The following assumptions are needed in the analysis.

Assumption 1. (i) The model operator \mathcal{M}_t is Lipschitz continuous, that is $\|\mathcal{M}_t(\mathbf{x}) - \mathcal{M}_t(\mathbf{x}')\| \leq \ell_0 \|\mathbf{x} - \mathbf{x}'\|$ for any $\mathbf{x}, \mathbf{x}' \in R^p$ for a positive constant ℓ_0 . (ii) The model operator \mathcal{M}_t can be locally linearized and satisfies $\|\mathcal{M}_t(\mathbf{x}) - \mathcal{M}_t(\mathbf{x}')\| \leq \|\dot{\mathcal{M}}_t\| \|\mathbf{x} - \mathbf{x}'\|$ for $\mathbf{x}, \mathbf{x}' \in R^p$ and $\|\mathbf{x} - \mathbf{x}'\| \leq \|\mathbf{h}\|$ for a small positive \mathbf{h} , where $\dot{\mathcal{M}}_t$ is a matrix related to the linear expansion of \mathcal{M}_t at \mathbf{x} and $\|\dot{\mathcal{M}}_t\| \leq \ell_t$ for some positive constants ℓ_t .

Assumption 2. The model error covariance \mathbf{Q}_t , the observation error covariance \mathbf{R}_t and the initial analysis covariance Σ_0^a satisfy $0 < \varepsilon_0 \leq \lambda_{\min}(\mathbf{Q}_t) \leq \lambda_{\max}(\mathbf{Q}_t) \leq 1/\varepsilon_0$, $0 < \varepsilon_0 \leq \lambda_{\min}(\mathbf{R}_t) \leq \lambda_{\max}(\mathbf{R}_t) \leq 1/\varepsilon_0$, and $\lambda_{\max}(\Sigma_0^a) \leq 1/\varepsilon_0$, for a positive ε_0 , respectively, where λ_{\max} and λ_{\min} are the maximum and minimum eigenvalue operators, respectively.

Assumption 3. The observation operator \mathbf{H}_t satisfies $\|\mathbf{H}_t\| \leq C$ for a constant $C > 0$.

Assumption 1 (i) and (ii) are two versions of the condition on the model operator \mathcal{M}_t . If model \mathcal{M}_t is linear, it automatically satisfies both (i) and (ii) of Assumption 1. If \mathcal{M}_t is nonlinear and Lipschitz continuous, $\mathcal{M}_t(\cdot)$ has at most linear growth at infinite intervals. However, strongly nonlinear systems may not satisfy the Lipschitz condition. In that case, we assume \mathcal{M}_t satisfies condition (ii), which is related to the tangent linear hypothesis (Thepaut and Courtier, 1991; Bouttier and Courtier, 1999) in the 4D-Var, where \mathcal{M}_t is determined in the linear approximation $\mathcal{M}_t(\mathbf{x}_t + \mathbf{h}) \approx \mathcal{M}_t(\mathbf{x}_t) + \dot{\mathcal{M}}_t \mathbf{h}$ in the vicinity of \mathbf{x}_t for

a perturbation \mathbf{h} , and the operator \dot{M}_t is called the differential or tangent linear function of \mathcal{M}_t at point \mathbf{x}_t . Assumption 2 assumes the eigenvalues of the three basic covariances \mathbf{Q}_t , \mathbf{R}_t and Σ_0^a are bounded away from zero and infinity. From Lemma S.3.1 of the SM, the eigenvalues of Σ_t^f satisfy the conditions for the thresholding and bandable(or circular bandable) covariance classes under Assumption 2 and Assumptions 1-2, respectively. Assumption 3 puts a mild condition on the observation operator \mathbf{H}_t .

The following lemma provides a basic result that bounds $\|\hat{\mathbf{K}}_t - \mathbf{K}_t\|$ for both fixed and high dimensional situations, where $\hat{\mathbf{K}}_t = \hat{\Sigma}_t^f \mathbf{H}_t^T (\mathbf{H}_t \hat{\Sigma}_t^f \mathbf{H}_t^T + \mathbf{R}_t)^{-1}$ is an estimator of the Kalman Gain matrix assuming \mathbf{R}_t is known. Closely related forms have appeared in the literature (Le Gland et al., 2009; Kwiatkowski and Mandel, 2015).

Lemma 3.1. *Suppose \mathbf{R}_t is known and $\lambda_{\min}(\mathbf{R}_t) > 0$, then*

$$\|\hat{\mathbf{K}}_t - \mathbf{K}_t\| \leq \lambda_{\min}^{-1}(\mathbf{R}_t) \|\mathbf{I} - \mathbf{K}_t \mathbf{H}_t\| \|\mathbf{H}_t\| \|\hat{\Sigma}_t^f - \Sigma_t^f\| \leq \lambda_{\min}^{-1}(\mathbf{R}_t) \|\mathbf{H}_t\| \|\hat{\Sigma}_t^f - \Sigma_t^f\|.$$

Lemma 3.1 suggests that the upper bound of the estimation error in $\|\hat{\mathbf{K}}_t - \mathbf{K}_t\|$ mainly depends on the bound of $\|\hat{\Sigma}_t^f - \Sigma_t^f\|$, which is valid for both fixed and high dimensions. Note that under fixed dimension, the sample covariance is consistent with the underlying population covariance at the \sqrt{n} rate, that is $\|\hat{\Sigma}_t^f - \Sigma_t^f\| = O_P(n^{-1/2})$ and thus $\|\hat{\mathbf{K}}_t - \mathbf{K}_t\| = O_P(n^{-1/2})$. The corresponding results for the high dimensions are shown later.

Remark 1. The last inequality in Lemma 3.1 is derived from $\|\mathbf{I} - \mathbf{K}_t \mathbf{H}_t\| < 1$ as $(\mathbf{I} - \mathbf{K}_t \mathbf{H}_t) \Sigma_t^f = \Sigma_t^a$ is the conditional variance of $\mathbf{x}_t | \mathbf{y}_{1:t}$ and $(\mathbf{I} - \mathbf{K}_t \mathbf{H}_t) \Sigma_t^f = \Sigma_t^a < \Sigma_t^f$ as long as \mathbf{x}_t is correlated with $\mathbf{y}_{1:t}$. Let us take a close look at $\|\mathbf{I} - \mathbf{K}_t \mathbf{H}_t\|$. For the extreme case of $\mathbf{R}_t = \mathbf{0}$, $\|\mathbf{I} - \mathbf{K}_t \mathbf{H}_t\|$ would be 0 if \mathbf{H}_t is invertible. Intuitively, $\|\mathbf{I} - \mathbf{K}_t \mathbf{H}_t\|$ would be close to 0 if \mathbf{R}_t is close to $\mathbf{0}$. Suppose $p = q = 1$, then $\|\mathbf{I} - \mathbf{K}_t \mathbf{H}_t\| = (1 + \mathbf{H}_t^2 \sigma_{\Sigma_t^f}^2 / \sigma_{\mathbf{R}_t}^2)^{-1} < 1$. This means that $\|\mathbf{I} - \mathbf{K}_t \mathbf{H}_t\|$ decreases with the increase of $\mathbf{H}_t^2 \sigma_{\Sigma_t^f}^2$ or decrease of $\sigma_{\mathbf{R}_t}^2$. For $p, q > 1$, if $\mathbf{H}_t = \mathbf{I}$, then $\|\mathbf{I} - \mathbf{K}_t \mathbf{H}_t\| = \|\mathbf{I} - \Sigma_t^f (\Sigma_t^f + \mathbf{R}_t)^{-1}\| = \varepsilon_0^2 / (1 + \varepsilon_0^2)$ if we assume

$\mathbf{R}_t = \varepsilon_0^2 \Sigma_t^f$. This means that $\|\mathbf{I} - \mathbf{K}_t \mathbf{H}_t\|$ will decrease with the decrease of ε_0^2 , the ratio of \mathbf{R}_t to Σ_t^f .

In practice, the true observation error covariance matrix \mathbf{R}_t may be unknown. Let $\hat{\mathbf{R}}_t$ be an estimator of \mathbf{R}_t based on either knowledge or historical data. The following Corollary 3.1 provides a result that bounds $\|\hat{\mathbf{K}}_t - \mathbf{K}_t\|$ for both fixed and high dimensional situations, where $\hat{\mathbf{K}}_t = \hat{\Sigma}_t^f \mathbf{H}_t^T (\mathbf{H}_t \hat{\Sigma}_t^f \mathbf{H}_t^T + \hat{\mathbf{R}}_t)^{-1}$ is an estimator of the Kalman Gain matrix when both the forecast and observation error covariance matrices Σ_t^f and \mathbf{R}_t are estimated by $\hat{\Sigma}_t^f$ and $\hat{\mathbf{R}}_t$, respectively.

Corollary 3.1. *If both the forecast and observation error covariance matrices Σ_t^f and \mathbf{R}_t are estimated by $\hat{\Sigma}_t^f$ and $\hat{\mathbf{R}}_t$, respectively, then*

$$\|\hat{\mathbf{K}}_t - \mathbf{K}_t\| \leq (\|\mathbf{I} - \mathbf{K}_t \mathbf{H}_t\| \|\hat{\Sigma}_t^f - \Sigma_t^f\| \|\mathbf{H}_t\| + \|\mathbf{K}_t\| \|\mathbf{R}_t - \hat{\mathbf{R}}_t\|) \|(\mathbf{H}_t \hat{\Sigma}_t^f \mathbf{H}_t^T + \hat{\mathbf{R}}_t)^{-1}\|.$$

If \mathbf{R}_t is invertible and $\hat{\mathbf{R}}_t$ is invertible with probability approaching 1, then

$$\|\hat{\mathbf{K}}_t - \mathbf{K}_t\| \leq \lambda_{\min}^{-1}(\hat{\mathbf{R}}_t) \|\mathbf{H}_t\| \|\hat{\Sigma}_t^f - \Sigma_t^f\| + \lambda_{\min}^{-1}(\hat{\mathbf{R}}_t) \lambda_{\min}^{-1}(\mathbf{R}_t) \|\mathbf{H}_t\| \|\Sigma_t^f\| \|\mathbf{R}_t - \hat{\mathbf{R}}_t\|.$$

Compared with the upper bound in Lemma 3.1, there is an extra term related to the bound of the estimation error in the observation error covariance matrix \mathbf{R}_t . Most of the results established in the following of the paper are for the case of known \mathbf{R}_t as is commonly assumed in the literature of the EnKF. Results for estimated \mathbf{R}_t can be attained in the fashion shown in Corollary 3.1.

Based on the result in Lemma 3.1 (or Corollary 3.1 for unknown \mathbf{R}_t), we can establish the convergence of the EnKF forecast and analysis states $\hat{\mathbf{x}}_t^f$ and $\hat{\mathbf{x}}_t^a$ to their oracle Kalman Filter counterparts \mathbf{x}_t^f and \mathbf{x}_t^a based on the true Σ_t^f and the true underlying evolution given in (2.4)-(2.5) by firstly establishing the convergence of $\hat{\Sigma}_t^f$ to Σ_t^f . For the fixed or low

dimensional state vectors \mathbf{x}_t where p is of a smaller order of the ensemble size n such that $p/n \rightarrow 0$, the sample covariance matrix is consistent such that $\|\hat{\Sigma}_t^f - \Sigma_t^f\| = O_P(n^{-1/2})$.

However, remote sensing technology has been advancing the measurement of massive amounts of data sets for many geophysical processes, which produces high resolution observational data. Meanwhile, the increasing demands of high resolution forecast and dataset also make the spatiotemporal resolution of the state variables become much higher. Both make \mathbf{x}_t high dimensional and bring high dimensional challenges on the validity of the EnKF. When the dimension p of the state vector \mathbf{x}_t is high so that $p \gg n$, the forecast ensemble sample covariance $\hat{\Sigma}_t^f$ in (2.8) is no longer consistent to the underlying covariance Σ_t^f (Bai and Yin, 1993), which is a major threat to the validity of the EnKF. The last two decades have witnessed rapid development in high dimensional statistical inference. Consistent high dimensional covariance estimators have been proposed, which include the banding, tapering and thresholding estimators (Bickel and Levina, 2008b,a; Cai et al., 2010).

Next, we present several consistent estimators of the high dimensional forecast error covariance Σ_t^f and their covariance classes before we evaluate the accuracy of the high dimensional assimilated state $\hat{\mathbf{x}}_t^a$ from the EnKF to the underlying \mathbf{x}_t^a of the Kalman Filter.

3.1 Consistent estimation of high dimensional forecast error covariance matrix

The banding estimator (Bickel and Levina, 2008b) of the forecast error covariance matrix with bandwidth k is

$$B_k(\mathbf{S}_t^f) = [s_{tij}^f \mathbf{1}(|i - j| \leq k)]_{p \times p}, \quad 0 \leq k < p,$$

where $\mathbf{S}_t^f = [s_{tij}^f]_{p \times p}$ is the sample covariance of the EnKF forecast ensembles. The covariance matrix class suitable for the banding estimator is the following bandable covariance class, $\mathcal{U}_b(\varepsilon_0, \alpha, C) = \{\Sigma = (\sigma_{ij})_{p \times p} : \max_j \sum_{|i-j|>k} |\sigma_{ij}| \leq Ck^{-\alpha} \text{ for all } k > 0 \text{ and } 0 < \varepsilon_0 \leq \lambda_{\min}(\Sigma) \leq \lambda_{\max}(\Sigma) \leq 1/\varepsilon_0\}$ for some positive α , C and ε_0 . This bandable pattern is generally consistent with the dependence between variables observed at sites i and j in geoscience studies, as the dependence becomes weaker as the distance between the two sites gets larger.

The banding estimator administers a hard threshold as it sets all matrix elements beyond the k -th sub-diagonals to zero. [Cai et al. \(2010\)](#) updated it with a tapering alteration which tapers down the level of the thresholding gradually

$$\hat{\Sigma}_{t,tap}^f(k) = \mathbf{S}_t^f \circ \mathbf{W}(k) = [w_{ij}(k)s_{tij}^f]_{p \times p},$$

where $\mathbf{W}(k) = (w_{ij}(k))_{p \times p}$, with $w_{ij}(k) = (2/k)\{(k - |i - j|)_+ - (k/2 - |i - j|)_+\}$, is the tapering matrix at a tapering width k which is usually an even integer and $1 \leq k \leq p$.

In earth science, due to the largely spherical shape of the earth, for a study region that encompasses the entire earth or its poles, the state vectors are highly dependent for the variable components between the two ends of the state vector. Thus we propose a circular form of the bandable structure, $\mathcal{U}_{bc}(\varepsilon_0, \alpha, C) = \{\Sigma = (\sigma_{ij})_{p \times p} : \max_j \sum_{k_1 < |i-j| < p - k_2} |\sigma_{ij}| \leq C(k_1 + k_2)^{-\alpha} \text{ for all } 0 < k_1, k_2 < p \text{ and } 0 < \varepsilon_0 \leq \lambda_{\min}(\Sigma) \leq \lambda_{\max}(\Sigma) \leq 1/\varepsilon_0\}$. Figure 1 depicts the $h(k)$ functions and heatmaps of two specific covariances that belong to the two bandable covariance classes \mathcal{U}_b and \mathcal{U}_{bc} , where $h(k)$ is the average of the squares of the k^{th} subdiagonal entries of a covariance defined by $h(k) := 0.5(p - k)^{-1} \sum_{|l_1 - l_2|=k} \sigma_{l_1 l_2}^2 = (p - k)^{-1} \sum_{l=1}^{p-k} \sigma_{l, l+k}^2$. Figures 1 (a)-(b) show that the $h(k)$ functions of covariances in \mathcal{U}_b and \mathcal{U}_{bc} are L -type and U -type curves as the subdiagonal index k increases, respectively. For covariances in the circular bandable class $\mathcal{U}_{bc}(\varepsilon_0, \alpha, C)$, the proposed mid-banding forecast

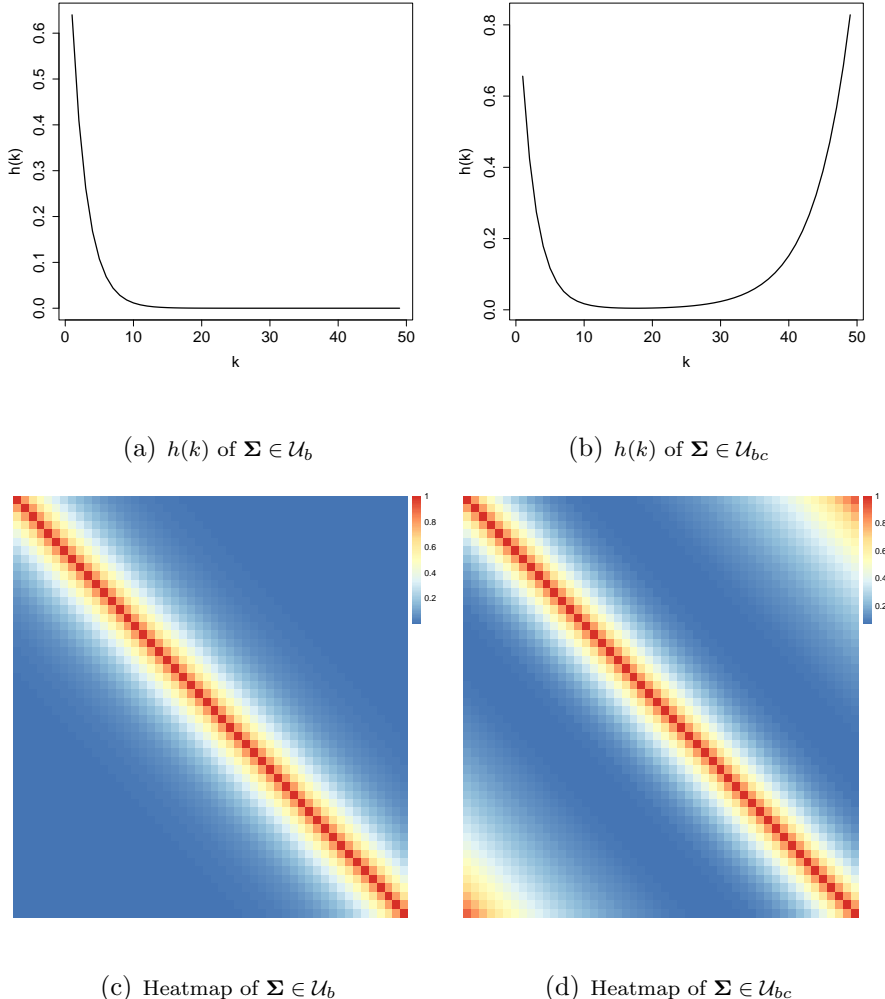


Figure 1: Bandable \mathcal{U}_b and circular bandable \mathcal{U}_{bc} covariance matrices: the average energy function $h(k)$ in Panels (a) and (b) and their heatmaps in Panels (c) and (d), where $h(k)$ is the average of the squares of the k^{th} sub-diagonal entries.

error covariance estimator with bandwidths k_1 and k_2 is

$$B_{k_1, k_2}(\mathbf{S}_t^f) = [s_{tij}^f \mathbf{1}(|i - j| \leq k_1 \text{ or } |i - j| \geq (p - k_2))]_{p \times p}, \quad 0 \leq k_1 < (p - k_2) \leq p.$$

The bandable matrix class requires that the state vector \mathbf{x}_t has an ordering (or a permutation) such that the correlation decays as two components of \mathbf{x}_t are further apart. However, the presence of geo-spatial processes (weather front or hurricane) and geography (mountains or ocean) will interrupt the spatial dependence ordering prescribed by the banding covariance class. In such situations, the thresholding covariance class $\mathcal{U}_\tau(\gamma, c_0(p), M, \varepsilon_0)$

suitable for the thresholding estimator (Bickel and Levina, 2008a) may be employed, where

$$\mathcal{U}_\tau(\gamma, c_0(p), M, \varepsilon_0) = \left\{ \boldsymbol{\Sigma} = (\sigma_{ij})_{p \times p} : \sigma_{ii} \leq M, \sum_{j=1}^p |\sigma_{ij}|^\gamma \leq c_0(p), \text{ for all } i \text{ and } \lambda_{\min}(\boldsymbol{\Sigma}) \geq \varepsilon_0 > 0 \right\}, \text{ for } 0 \leq \gamma < 1. \text{ The thresholding forecast error covariance matrix estimator with a threshold level } s \text{ is } T_s(\mathbf{S}_t^f) = [s_{tij}^f \mathbf{1}(|s_{tij}^f| \geq s)]_{p \times p}.$$

Note that all of the banding, mid-banding, tapering and thresholding estimators depend on either the bandwidth k or the threshold s which can be selected by methods in Qiu and Chen (2015). For the bandwidths k_1, k_2 of the mid-banding estimator, we propose a similar selection method and details can be found in Section S.2 of the SM.

To apply the high dimensional estimators of the forecasting error covariance $\boldsymbol{\Sigma}_t^f$, we need the following distributional assumption.

Assumption 4. The random vectors $\mathbf{x}_{t,i}^f = (x_{t,i1}^f, \dots, x_{t,ip}^f)^\top$ are IID and each $x_{t,1j}^f \stackrel{d}{\sim} F_{t,j}$ and $(x_{t,1j}^f)^2 \stackrel{d}{\sim} G_{t,j}$, where $G_{t,j}(u) = F_{t,j}(\sqrt{u}) - F_{t,j}(-\sqrt{u})$ for $u > 0$. There exists a $\lambda_0 > 0$ such that $\max_{1 \leq j \leq p} \mathbb{E}(e^{\lambda(x_{t,1j}^f)^2}) < \infty$ for $\lambda \in (-\lambda_0, \lambda_0)$.

Assumption 4 effectively assume $(x_{t,1j}^f)^2$ are sub-exponentially distributed, which include the Sub-Gaussian random variables as a special case.

The following Proposition 3.1 summarizes the convergence rates of the forecast error covariance estimators by the banding, mid-banding, tapering and thresholding methods.

Proposition 3.1. *Suppose the forecast ensemble $\{\mathbf{x}_{ti}^f\}_{i=1}^n$ are conditionally sub-exponentially distributed as in Assumption 4.*

(i) *For the banding estimator $B_k(\mathbf{S}_t^f)$ with $k \asymp (n^{-1} \log p)^{-1/(2\alpha+2)}$, then uniformly for*

$$\boldsymbol{\Sigma}_t^f \in \mathcal{U}_b(\varepsilon_0, \alpha, C), \mathbb{E}\|B_k(\mathbf{S}_t^f) - \boldsymbol{\Sigma}_t^f\|^2 \asymp (n^{-1} \log p)^{\alpha/(\alpha+1)}.$$

(ii) *For the mid-banding estimator $B_{k_1, k_2}(\mathbf{S}_t^f)$ with $k_1 + k_2 \asymp (n^{-1} \log p)^{-1/(2\alpha+2)}$, uniformly*

$$\text{on } \boldsymbol{\Sigma}_t^f \in \mathcal{U}_{bc}(\varepsilon_0, \alpha, C), \mathbb{E}\|B_{k_1, k_2}(\mathbf{S}_t^f) - \boldsymbol{\Sigma}_t^f\|^2 \asymp (n^{-1} \log p)^{\alpha/(\alpha+1)}.$$

(iii) For the tapering estimator $\hat{\Sigma}_{t,tap}^f(k)$ and $\Sigma_t^f \in \mathcal{U}_b(\varepsilon_0, \alpha, C)$, the optimal rate of convergence of the tapering estimator is $\mathbb{E}\|\hat{\Sigma}_{t,tap}^f(k) - \Sigma_t^f\|^2 \asymp \min\{n^{-2\alpha/(2\alpha+1)} + n^{-1}\log p, n^{-1}p\}$.

(iv) For the thresholding estimator $T_s(\mathbf{S}_t^f)$, for sufficiently large M' , if $s = M'(n^{-1}\log p)^{-1/2}$, then, uniformly on $\mathcal{U}_\tau(\gamma, c_0(p), M)$, $\mathbb{E}\|T_s(\mathbf{S}_t^f) - \Sigma_t^f\|^2 \asymp c_0^2(p)(n^{-1}\log p)^{(1-\gamma)}$.

The results in Proposition 3.1 (i), (iii) and (iv) are, respectively, from [Bickel and Levina \(2008b\)](#), [Cai et al. \(2010\)](#) and [Bickel and Levina \(2008a\)](#). And that for the mid-banding estimator in Proposition 3.1 (ii) is a new result whose proof is given in the SM. They imply that the high dimensional covariance estimators are consistent to Σ_t^f under the spectral norm if $\log(p) = o(n)$ or $p = o(e^{cn})$ for any positive constant c .

According to Lemma 3.1, the convergence results in Proposition 3.1 on the high dimensional estimation of Σ_t^f translate to that of the estimated Kalman Gain $\hat{\mathbf{K}}_t = \hat{\Sigma}_t^f \mathbf{H}_t^T (\mathbf{H}_t \hat{\Sigma}_t^f \mathbf{H}_t^T + \mathbf{R}_t)^{-1}$ to \mathbf{K}_t . Specifically,

$$\begin{aligned}
& \text{if } \Sigma_t^f \in \mathcal{U}_b(\varepsilon_0, \alpha, C) \text{ or } \mathcal{U}_{bc}(\varepsilon_0, \alpha, C), \mathbb{E}\|\hat{\mathbf{K}}_t - \mathbf{K}_t\|^2 \asymp \left(\frac{\log p}{n}\right)^{\frac{\alpha}{\alpha+1}} \text{ for } \hat{\Sigma}_t^f = B_k(\mathbf{S}_t^f) \text{ or } B_{k_1, k_2}(\mathbf{S}_t^f); \\
& \text{if } \Sigma_t^f \in \mathcal{U}_b(\varepsilon_0, \alpha, C), \mathbb{E}\|\hat{\mathbf{K}}_t - \mathbf{K}_t\|^2 \asymp \min\left\{n^{\frac{-2\alpha}{2\alpha+1}} + \frac{\log p}{n}, \frac{p}{n}\right\} \text{ for } \hat{\Sigma}_t^f = \hat{\Sigma}_{t,tap}^f(k); \\
& \text{if } \Sigma_t^f \in \mathcal{U}_\tau(\gamma, c_0(p), M), \mathbb{E}\|\hat{\mathbf{K}}_t - \mathbf{K}_t\|^2 \asymp c_0^2(p)\left(\frac{\log p}{n}\right)^{(1-\gamma)} \text{ for } \hat{\Sigma}_t^f = T_s(\mathbf{S}_t^f). \tag{3.1}
\end{aligned}$$

As will be shown later, the Kalman Gain estimation error $\Delta_{\mathbf{K},t} = \mathbb{E}\|\hat{\mathbf{K}}_t - \mathbf{K}_t\|^2$ plays a crucial role in quantifying the effects of the high dimensional banding, mid-banding, tapering and thresholding estimators for Σ_t^f .

3.2 Convergence of High Dimensional Ensemble Kalman Filter

When the dimension p of \mathbf{x}_t is high, to allow consistency of the data assimilation, we have to use the high dimensional covariance estimators in Section 3.1 for the forecast error covariance matrix Σ_t^f and the Kalman Gain matrix \mathbf{K}_t . Based on the consistent estimators

of Σ_t^f and \mathbf{K}_t , we propose the HD-EnKF algorithms given in Section S.1 of the SM and we establish the accuracy of the assimilated state $\hat{\mathbf{x}}_t^a$ to the underlying \mathbf{x}_t^a in the following. To simplify notation, we denote $\Delta_{\mathbf{K},k} = \mathbb{E}\|\hat{\mathbf{K}}_k - \mathbf{K}_k\|^2$ and

$$\begin{aligned}\Omega_t = & \text{tr} \left(n^{-1} \mathbb{E}(\hat{\mathbf{K}}_t - \mathbf{K}_t)^T (\hat{\mathbf{K}}_t - \mathbf{K}_t) (\mathbf{H}_t \Sigma_t^f \mathbf{H}_t^T + \mathbf{R}_t) \right) + \mathbb{E}\|(\hat{\mathbf{K}}_t - \mathbf{K}_t)(\mathbf{y}_t - \mathbf{H}_t \mathbf{x}_t^f)\|^2 \\ & - 2 \text{tr} \left((\mathbf{I} - \mathbf{K}_t \mathbf{H}_t)^T \mathbb{E}(\hat{\mathbf{K}}_t - \mathbf{K}_t) \mathbf{H}_t \Sigma_t^f / n \right) + 2 \text{tr} \left((\mathbf{K}_t^T \mathbb{E}(\hat{\mathbf{K}}_t - \mathbf{K}_t) \mathbf{R}_t / n) \right).\end{aligned}$$

The following Theorem 3.1 presents the upper bounds of the discrepancy between the EnKF analysis state and the underlying Kalman Filter analysis for the one-step data assimilation for a general case where the model operator \mathcal{M}_t is possibly nonlinear.

Theorem 3.1. *Suppose Assumptions 1(i) or 1(ii), 2, 3 hold and the forecast ensemble $\{\mathbf{x}_{t,j}^f\}_{j=1}^n$ are independently sampled from the distribution of $\mathbf{x}_t \mid \mathbf{y}_{1:t-1}$ with mean \mathbf{x}_t^f and covariance Σ_t^f . Then, the forecast and analysis states of the EnKF at time t satisfy*

$$\begin{aligned}p^{-1} \mathbb{E}\{\|\hat{\mathbf{x}}_t^f - \mathbf{x}_t^f\|^2 \mid \mathbf{y}_{1:t-1}\} &= n^{-1} p^{-1} \text{tr}(\Sigma_t^f) = O(n^{-1}), \\ p^{-1} \mathbb{E}\{\|\hat{\mathbf{x}}_t^a - \mathbf{x}_t^a\|^2 \mid \mathbf{y}_{1:t}\} &= \text{tr} \left(n^{-1} p^{-1} (\mathbf{I} - \mathbf{K}_t \mathbf{H}_t) \Sigma_t^f \right) + p^{-1} \Omega_t \\ &= O(n^{-1} + p^{-1} \Delta_{\mathbf{K},t} \|\mathbf{y}_t - \mathbf{H}_t \mathbf{x}_t^f\|^2).\end{aligned}\tag{3.2}$$

Theorem 3.1 gives the upper bounds of the one-step data assimilation MSE with high dimensional forecast error covariance estimators, which depends on $\Delta_{\mathbf{K},t}$ whose convergence rates for different covariance estimators are given in (3.1). Note that the first term in (3.2), $n^{-1}(\mathbf{I} - \mathbf{K}_t \mathbf{H}_t) \Sigma_t^f = n^{-1} \Sigma_t^a$, is the variance of the sample mean of the analysis ensemble using the true forecast error covariance Σ_t^f and the second term Ω_t results from the estimation error of $\hat{\Sigma}_t^f$. Specifically, with the banding or mid-banding estimators, the tapering estimator and the thresholding estimator, the one-step EnKF data assimilation

MSE are, respectively,

$$p^{-1}\mathbb{E}\{\|\hat{\mathbf{x}}_t^a - \mathbf{x}_t^a\|^2 | \mathbf{y}_{1:t}\} \asymp \max\{n^{-1}, p^{-1}q(n^{-1}\log p)^{\alpha/(\alpha+1)}\}, \quad (3.3)$$

$$p^{-1}\mathbb{E}\{\|\hat{\mathbf{x}}_t^a - \mathbf{x}_t^a\|^2 | \mathbf{y}_{1:t}\} \asymp \max\{n^{-1}, p^{-1}q(n^{\frac{-2\alpha}{2\alpha+1}} + n^{-1}\log p)\}, \quad (3.4)$$

$$p^{-1}\mathbb{E}\{\|\hat{\mathbf{x}}_t^a - \mathbf{x}_t^a\|^2 | \mathbf{y}_{1:t}\} \asymp \max\{n^{-1}, p^{-1}qc_0^2(p)(n^{-1}\log p)^{(1-\gamma)}\}. \quad (3.5)$$

It should also be noted that the above results are valid for general model operators \mathcal{M}_t given in Assumption 1-(i) and (ii). Compared with the results in [Al-Ghattas and Sanz-Alonso \(2024\)](#), they investigated the difference between the ensembles of single-step Ensemble Kalman Inversion using the localized estimation and the true forecast error covariance matrices, under the framework of the effective dimension of a matrix \mathbf{A} defined by $\text{tr}(\mathbf{A})/\|\mathbf{A}\|$ (or the max-log effective dimension for a sparse covariance).

For fixed p, q , both the forecast and analysis states of the EnKF converge to the underlying forecast and analysis states of the Kalman Filter with a convergence rate of \sqrt{n} as $n \rightarrow \infty$ because $\Delta_{\mathbf{K},t} = O(n^{-1})$, as also shown in Theorem S.3.1 of the SM. Furthermore, for linear model operator \mathbf{M}_t , Proposition S.3.1 of the SM implies that with Gaussian initial state, the asymptotic conditional distributions of the analysis ensemble $\mathbf{x}_{t,j}^a | \mathbf{y}_{1:t}$ and the forecast ensemble $\mathbf{x}_{t,j}^f | \mathbf{y}_{1:t-1}$ in the EnKF are the same as those of $\mathbf{x}_t | \mathbf{y}_{1:t}$ and $\mathbf{x}_t | \mathbf{y}_{1:t-1}$ in the Kalman Filter, respectively.

To show the impact of the dimensionality on the assimilation MSE, we take the banding and mid-banding estimators as examples. If $q \asymp p$, $p^{-1}\mathbb{E}\{\|\hat{\mathbf{x}}_t^a - \mathbf{x}_t^a\|^2 | \mathbf{y}_{1:t}\} = O((n^{-1}\log p)^{2\alpha/(2\alpha+2)})$, which implies that the one-step assimilation MSE mainly depends on the estimation error of the Kalman Gain. Commonly in high resolution data assimilation, the dimension of the observation \mathbf{y}_t is much smaller than that of the state vector \mathbf{x}_t , so that $q \ll p$. If q is relatively large such that $p^{-1}q(n^{-1}\log p)^{\alpha/(\alpha+1)} \gg n^{-1}$, then the estimation error of the Kalman Gain matrix will dominate, that is, $p^{-1}\mathbb{E}\{\|\hat{\mathbf{x}}_t^a - \mathbf{x}_t^a\|^2 | \mathbf{y}_{1:t}\} = O(p^{-1}q(n^{-1}\log p)^{\alpha/(\alpha+1)})$. Other-

wise, the first term n^{-1} dominates. However, if sample covariance \mathbf{S}_t^f is used in $\hat{\mathbf{K}}_t$ when $p \geq n$, then $p^{-1}\mathbb{E}\{\|\hat{\mathbf{x}}_t^a - \mathbf{x}_t^a\|^2|\mathbf{y}_{1:t}\} = O(p/n^2\|\mathbf{y}_t - \mathbf{H}_t\mathbf{x}_t^f\|^2) = O(pq/n^2)$. For the impact of the observation dimension q on the MSE, a study in the SM shows that if the additional observation $y_{t,q+1}$ is not far away from its forecast $\mathbf{H}_t\mathbf{x}_t^f$, the MSE will decrease since the first term in (3.2) decreases more.

For the discrepancies between the EnKF analysis state and the true state, as $\mathbb{E}\{\|\hat{\mathbf{x}}_t^a - \mathbf{x}_t\|^2|\mathbf{y}_{1:t}\} = \mathbb{E}\{\|\hat{\mathbf{x}}_t^a - \mathbf{x}_t^a\|^2|\mathbf{y}_{1:t}\} + \mathbb{E}\{\|\mathbf{x}_t^a - \mathbf{x}_t\|^2|\mathbf{y}_{1:t}\}$ and \mathbf{x}_t is a random variable with $\mathbb{E}\{\|\mathbf{x}_t^a - \mathbf{x}_t\|^2|\mathbf{y}_{1:t}\} = \text{tr}(\Sigma_t^a)$ which is a constant not related to the ensemble size n for a fixed p , then $\mathbb{E}\{\|\hat{\mathbf{x}}_t^a - \mathbf{x}_t\|^2|\mathbf{y}_{1:t}\}$ can not converge to zero. This is due to the fact that the underlying state is a random variable. In contrast, \mathbf{x}_t^a is a conditional mean and is possible to be estimated consistently.

In practice, the ensemble forecast-analysis process in the EnKF repeats for multiple time steps ahead to make longer-time predictions. Thus, in addition to the one-step ahead data assimilation accuracy, one may also care about the quality of multiple-step forecasting and analysis. The following Theorem 3.2 gives the h -step MSE bounds between the forecast/analysis states of the EnKF in comparison to the underlying Kalman Filters. To simplify writing, define two non-stochastic constants

$$C_{t,h}^A = \frac{1 - L_{t,h}^h A_{t,h}^h}{1 - L_{t,h} A_{t,h}} \text{ and } C_{t,h}^B = \frac{1 - L_{t,h}^h B_{t,h}^h}{1 - L_{t,h} B_{t,h}}, \quad (3.6)$$

where $A_{t,h} = \max_{t < k \leq t+h} \|\mathbf{I} - \mathbf{K}_k \mathbf{H}_k\|$, $B_{t,h} = \max_{t < k \leq t+h} \{\mathbb{E}\|\mathbf{I} - \hat{\mathbf{K}}_k \mathbf{H}_k\|\}$, and $L_{t,h} = \max_{0 < k \leq t+h} \{\ell_0, \ell_k\}$ with ℓ_0 and ℓ_k being respectively the Lipschitz coefficient and the upper bound of the local linearization coefficient of the model operation defined in Assumption 1. We further denote

$$U_k = \{\|\mathbf{y}_k - \mathbf{H}_k \mathbf{x}_k^f\|^2 \Delta_{\mathbf{K},k} + \text{tr}(\mathbb{E}(\hat{\mathbf{K}}_k - \mathbf{K}_k)^T (\hat{\mathbf{K}}_k - \mathbf{K}_k) (\mathbf{H}_k \Sigma_k^f \mathbf{H}_k^T + \mathbf{R}_k))\}^{1/2}.$$

Theorem 3.2. *Assumptions 1(i) or 1(ii), 2, 3 hold and the analysis ensemble $\{\mathbf{x}_{t,j}^a\}_{j=1}^n$ is generated independently from the distribution of $\mathbf{x}_t \mid \mathbf{y}_{1:t}$ with mean \mathbf{x}_t^a and covariance Σ_t^a at time t . By repeatedly performing the ensemble forecast-analysis process h steps, the forecast and analysis states of the EnKF at the time $t+h$ satisfy*

$$\begin{aligned} p^{-1}\mathbb{E}\{\|\hat{\mathbf{x}}_{t+h}^f - \mathbf{x}_{t+h}^f\|^2 \mid \mathbf{y}_{1:t+h-1}\} &\leq p^{-1}\left(\{\text{tr}(n^{-1}\Sigma_{t+h}^f)\}^{1/2} + L_{t,h}C_{t,h-1}^B \max_{t < k \leq t+h-1} U_k\right)^2 \\ &= O\left(n^{-1} + p^{-1}L_{t,h}^2(C_{t,h-1}^A)^2 \max_{t < k \leq t+h-1} \{\Delta_{\mathbf{K},k} \|\mathbf{y}_k - \mathbf{H}_k \mathbf{x}_k^f\|^2\}\right), \\ p^{-1}\mathbb{E}\|(\hat{\mathbf{x}}_{t+h}^a - \mathbf{x}_{t+h}^a) \mid \mathbf{y}_{1:t+h}\|^2 &\leq p^{-1}\left(\{\text{tr}(n^{-1}\Sigma_{t+h}^a)\}^{1/2} + C_{t,h}^B \max_{t < k \leq t+h} U_k\right)^2 \\ &= O\left(n^{-1} + p^{-1}(C_{t,h}^A)^2 \max_{t < k \leq t+h} \{\Delta_{\mathbf{K},k} \|\mathbf{y}_k - \mathbf{H}_k \mathbf{x}_k^f\|^2\}\right). \end{aligned}$$

Compared with the one-step results in Theorem 3.1, the term related to the estimation error in $\hat{\Sigma}_{t+k}^f$ in the h -step analysis MSE is inflated with constants $(C_{t,h}^A)^2$ which are related to $L_{t,h}$ and $A_{t,h}$ defined after (3.6). This is because of the accumulation of the estimation error of $\hat{\Sigma}_{t+k}^f$ in the data assimilation, which can be seen from the proof of Theorem 3.2 in the SM. Using a similar analysis on the one-step results after Theorem 3.1 and according to (3.1), the h -step assimilation MSE between the analysis state of the EnKF $\hat{\mathbf{x}}_{t+h}^a$ and the \mathbf{x}_{t+h}^a for Σ_t^f estimated by the four high dimensional estimators are, respectively,

$$p^{-1}\mathbb{E}\|(\hat{\mathbf{x}}_{t+h}^a - \mathbf{x}_{t+h}^a) \mid \mathbf{y}_{1:t+h}\|^2 \asymp \max\left\{n^{-1}, (C_{t,h}^A)^2 p^{-1} q(n^{-1} \log p)^{\alpha/(\alpha+1)}\right\}, \quad (3.7)$$

$$p^{-1}\mathbb{E}\|(\hat{\mathbf{x}}_{t+h}^a - \mathbf{x}_{t+h}^a) \mid \mathbf{y}_{1:t+h}\|^2 \asymp \max\left\{n^{-1}, (C_{t,h}^A)^2 p^{-1} q(n^{-\frac{2\alpha}{2\alpha+1}} + n^{-1} \log p)\right\}, \quad (3.8)$$

$$p^{-1}\mathbb{E}\|(\hat{\mathbf{x}}_{t+h}^a - \mathbf{x}_{t+h}^a) \mid \mathbf{y}_{1:t+h}\|^2 \asymp \max\left\{n^{-1}, (C_{t,h}^A)^2 p^{-1} q c_0^2(p) (n^{-1} \log p)^{(1-\gamma)}\right\}, \quad (3.9)$$

in which the estimation error of \mathbf{K}_k are inflated by $(C_{t,h}^A)^2$ compared with that in the upper bound of the one-step assimilation MSE given in (3.3) - (3.5) in Theorem 3.1. According to Remark 1, $A_{t,h} = \max_{t < k \leq t+h} \|\mathbf{I} - \mathbf{K}_k \mathbf{H}_k\| < 1$. If $L_{t,h} A_{t,h} < 1$, then $C_{t,h}^A$ converges to a small constant and $L_{t,h}^h A_{t,h}^h \rightarrow 0$ as $h \rightarrow \infty$, although $C_{t,h}^A$ becomes larger along with the increase of h . Thus, $\mathbb{E}\{\|\hat{\mathbf{x}}_{t+h}^a - \mathbf{x}_{t+h}^a\|^2 \mid \mathbf{y}_{1:t+h}\} \asymp \mathbb{E}\{\|\hat{\mathbf{x}}_t^a - \mathbf{x}_t^a\|^2 \mid \mathbf{y}_{1:t}\}$. If $L_{t,h} A_{t,h} > 1$, then

$C_{t,h}^A$ increases a lot with the increase of h , which suggests the quality of the data assimilation deteriorates as h increases, although $\mathbb{E}\{\|\hat{\mathbf{x}}_{t+h}^a - \mathbf{x}_{t+h}^a\|^2 | \mathbf{y}_{1:t+h}\} \asymp \mathbb{E}\{\|\hat{\mathbf{x}}_t^a - \mathbf{x}_t^a\|^2 | \mathbf{y}_{1:t}\}$ for a fixed h . However, it is possible to make $L_{t,h}$ be smaller by shortening the forecast time step or the integration time step. This underscores the necessity of the high-quality or high dimensional estimators of the forecast error covariance, considering the accumulation of estimation errors in multiple-step data assimilation. The MSE between the forecast state of the EnKF $\hat{\mathbf{x}}_{t+h}^f$ and the Kalman Filter \mathbf{x}_{t+h}^f for the banding, mid-banding, tapering and thresholding estimators of Σ_t^f are similar to (3.7)-(3.9) but with slightly different inflation constants.

Sometimes, the assimilation process proceeds every k time steps not every step as one may not have observations at each step or the assimilation in every step is too computationally consuming. Theorem S.3.2 of the SM gives the MSE bounds for multiple-step forecasting and assimilation where the assimilation process proceeds every k time steps.

4 Imperfect Models

In practice, the exact form of the model operator \mathcal{M}_t is likely unknown, and the state-of-the-art model $\hat{\mathcal{M}}_t$ is only an approximation to \mathcal{M}_t . Besides, large dynamic models in earth science are often nonlinear, one may use its linear approximation (Julier and Uhlmann, 1997; Stroud et al., 2010). This section is devoted to quantifying the effects of the model approximation error on the accuracy of the analysis and forecast states of the EnKF. The following assumption regulates the extent of the model approximation error.

Assumption 5. Let $\xi_t = \hat{\mathcal{M}}_t(\mathbf{x}) - \mathcal{M}_t(\mathbf{x})$ be the error of the approximated model $\hat{\mathcal{M}}_t$ to \mathcal{M}_t with $\mathbb{E}(\xi_t) = \mu_{\xi_t}$ and $\text{Var}(\xi_t) = \Xi_{\xi_t}$. It is assumed that $\|\mu_{\xi_t}\|_{\infty} \leq C_1$ and $\|\Xi_{\xi_t}\| \leq C_2$ for some positive constants C_1 and C_2 .

Theorem 4.1 gives the one-step assimilation bounds of the difference between the forecast/analysis states of the EnKF and the Kalman Filter when \mathcal{M}_t is unknown. Denote

$$\begin{aligned}
V_t &= \text{tr} \left(n^{-1} (\mathbf{I} - \mathbf{K}_t \mathbf{H}_t)^T (\mathbf{I} - \mathbf{K}_t \mathbf{H}_t) \Xi_{\xi_t} \right) + \|(\mathbf{I} - \mathbf{K}_t \mathbf{H}_t) \mu_{\xi_t}\|^2 \\
&\quad + \text{tr} \left(n^{-1} \mathbb{E} (\hat{\mathbf{K}}_t - \mathbf{K}_t)^T (\hat{\mathbf{K}}_t - \mathbf{K}_t) (\mathbf{H}_t (\Sigma_t^f + \Xi_{\xi_t}) \mathbf{H}_t^T + \mathbf{R}_t) \right) \\
&\quad + \mathbb{E} \|(\hat{\mathbf{K}}_t - \mathbf{K}_t)(\mathbf{y}_t - \mathbf{H}_t \mathbf{x}_t^f - \mathbf{H}_t \mu_{\xi_t})\|^2 + 2 \text{tr} \left(\mathbf{K}_t^T \mathbb{E} (\hat{\mathbf{K}}_t - \mathbf{K}_t) \mathbf{R}_t / n \right) \\
&\quad - 2 \text{tr} \left((\mathbf{I} - \mathbf{K}_t \mathbf{H}_t)^T \mathbb{E} (\hat{\mathbf{K}}_t - \mathbf{K}_t) \{ \mathbf{H}_t (\Sigma_t^f + \Xi_{\xi_t}) / n + (\mathbf{y}_t - \mathbf{H}_t \mathbf{x}_t^f - \mathbf{H}_t \mu_{\xi_t}) \mu_{\xi_t}^T \} \right).
\end{aligned} \tag{4.1}$$

Theorem 4.1. Suppose Assumptions 1(i) or 1(ii), 2, 3, 5 hold and $\{\mathbf{x}_{t-1,j}^a\}_{j=1}^n$ is generated independently from the distribution of $\mathbf{x}_{t-1} \mid \mathbf{y}_{1:t-1}$ with mean \mathbf{x}_{t-1}^a and covariance Σ_{t-1}^a at time $t-1$. Then, if \mathcal{M}_t is approximated by $\hat{\mathcal{M}}_t$, the forecast and analysis states of the EnKF satisfy

$$p^{-1} \mathbb{E} \{ \|\hat{\mathbf{x}}_t^f - \mathbf{x}_t^f\|^2 \mid \mathbf{y}_{1:t-1} \} = n^{-1} p^{-1} \text{tr}(\Sigma_t^f + \Xi_{\xi_t}) + p^{-1} \|\mu_{\xi_t}\|^2, \tag{4.2}$$

$$\begin{aligned}
p^{-1} \mathbb{E} \{ \|\hat{\mathbf{x}}_t^a - \mathbf{x}_t^a\|^2 \mid \mathbf{y}_{1:t} \} &= p^{-1} \text{tr} \left(n^{-1} (\mathbf{I} - \mathbf{K}_t \mathbf{H}_t) \Sigma_t^f \right) + V_t \\
&= O \left(n^{-1} + p^{-1} \|(\mathbf{I} - \mathbf{K}_t \mathbf{H}_t) \mu_{\xi_t}\|^2 + p^{-1} \|\mathbf{y}_t - \mathbf{H}_t \mathbf{x}_t^f\|^2 (\|\Xi_{\xi_t}\|^2 + \tilde{\Delta}_{\mathbf{K},t}) \right)
\end{aligned} \tag{4.3}$$

where $\tilde{\Delta}_{\mathbf{K},t} = \mathbb{E} \|\tilde{\mathbf{K}}_t - \mathbf{K}_t\|^2$ and $\tilde{\mathbf{K}}_t$ is the estimated \mathbf{K}_t with true model \mathcal{M}_t .

The theorem suggests that the model approximation error creates extra terms related to μ_{ξ_t} and $\|\Xi_{\xi_t}\|$, which are absent from the results in Theorem 3.1 where accurate model is assumed. Specifically, the assimilation MSEs for fixed p, q and $p, q \rightarrow \infty$ are, respectively,

$$\mathbb{E} \{ \|\hat{\mathbf{x}}_t^a - \mathbf{x}_t^a\|^2 \mid \mathbf{y}_{1:t} \} \asymp \max \{ n^{-1}, \|(\mathbf{I} - \mathbf{K}_t \mathbf{H}_t) \mu_{\xi_t}\|^2, \|\Xi_{\xi_t}\|^2 \} \tag{4.4}$$

$$p^{-1} \mathbb{E} \{ \|\hat{\mathbf{x}}_t^a - \mathbf{x}_t^a\|^2 \mid \mathbf{y}_{1:t} \} \asymp \max \{ n^{-1}, p^{-1} \|(\mathbf{I} - \mathbf{K}_t \mathbf{H}_t) \mu_{\xi_t}\|^2, p^{-1} q \tilde{\Delta}_{\mathbf{K},t}, p^{-1} q \|\Xi_{\xi_t}\|^2 \}.$$

If $\|\Xi_{\xi_t}\| \neq 0$ but $\mu_{\xi_t} = \mathbf{0}$, which means $\hat{\mathcal{M}}_t$ is unbiased to \mathcal{M}_t , then for fixed p and q ,

$$\mathbb{E} \{ \|\hat{\mathbf{x}}_t^a - \mathbf{x}_t^a\|^2 \mid \mathbf{y}_{1:t} \} = O \left(n^{-1} + \|\mathbf{y}_t - \mathbf{H}_t \mathbf{x}_t^f\|^2 (\|\Xi_{\xi_t}\|^2 + n^{-1}) \right) = O \left(n^{-1} + \|\Xi_{\xi_t}\|^2 \right). \tag{4.5}$$

Thus, if $\|\Xi_{\xi_t}\|^2 = O(n^{-1})$, then $\mathbb{E}\{\|\hat{\mathbf{x}}_t^a - \mathbf{x}_t^a\|^2 | \mathbf{y}_{1:t}\} = O(n^{-1})$, that is, the model approximation error does not alter the order of magnitude of the assimilation MSEs of the EnKF. However, if $n\|\Xi_{\xi_t}\|^2 \rightarrow \infty$, then $\mathbb{E}\{\|\hat{\mathbf{x}}_t^a - \mathbf{x}_t^a\|^2 | \mathbf{y}_{1:t}\} = O(\|\Xi_{\xi_t}\|^2)$, which means the model approximation error dominates the assimilation MSE. When $p, q \rightarrow \infty$, $p^{-1}\mathbb{E}\{\|\hat{\mathbf{x}}_t^a - \mathbf{x}_t^a\|^2 | \mathbf{y}_{1:t}\} \asymp \max\{n^{-1}, p^{-1}q\tilde{\Delta}_{\mathbf{K},t}, p^{-1}q\|\Xi_{\xi_t}\|^2\}$.

If $\hat{\mathcal{M}}_t$ is a biased approximation to \mathcal{M}_t so that $\mu_{\xi_t} \neq 0$, the approximation bias would also contribute to the MSE. Specifically, for either fixed p and q or $p, q \rightarrow \infty$, the MSEs in the analysis states of the EnKF are, respectively,

$$\begin{aligned} \mathbb{E}\{\|\hat{\mathbf{x}}_t^a - \mathbf{x}_t^a\|^2 | \mathbf{y}_{1:t}\} &\asymp \max\{n^{-1}, \|(\mathbf{I} - \mathbf{K}_t \mathbf{H}_t)\mu_{\xi_t}\|^2, \|\Xi_{\xi_t}\|^2\} \text{ and} \\ p^{-1}\mathbb{E}\{\|\hat{\mathbf{x}}_t^a - \mathbf{x}_t^a\|^2 | \mathbf{y}_{1:t}\} &\asymp \max\{n^{-1}, p^{-1}\|(\mathbf{I} - \mathbf{K}_t \mathbf{H}_t)\mu_{\xi_t}\|^2, p^{-1}q\tilde{\Delta}_{\mathbf{K},t}, p^{-1}q\|\Xi_{\xi_t}\|^2\}. \end{aligned} \quad (4.6)$$

The above analysis shows that for both the fixed and diverging dimensions and both the unbiased and biased approximation of \mathcal{M}_t , the approximation errors as represented by μ_{ξ_t} and $\|\Xi_{\xi_t}\|^2$ contributes substantially to the assimilation MSE, which suggests that a good approximation of the model operator is a significant aspect of data assimilation.

While this may be obvious, Theorem 4.1 describes exactly how it happens.

The accumulation of the model approximation error is more pronounced in the h -step assimilation MSEs as shown in Theorem 4.2 and more details of the h -step assimilation in the presence of the model error can be found in Theorem S.3.4 of the SM. Define $D_{t,h} = \max_{t < k \leq t+h} \|\mathbf{I} - \check{\mathbf{K}}_k \mathbf{H}_k\|$, where $\check{\mathbf{K}}_k = (\Sigma_k^f + \Xi_k) \mathbf{H}_k^T (\mathbf{H}_k (\Sigma_k^f + \Xi_{\xi_k}) \mathbf{H}_k^T + \mathbf{R}_k)^{-1}$, which is the underlying Kalman Gain matrix under the imperfect model. Denote a non-stochastic constant $C_{t,h}^D = (1 - L_{t,h}^h D_{t,h}^h) / (1 - L_{t,h} D_{t,h})$.

Theorem 4.2. *Suppose Assumptions 1(i) or 1(ii), 2, 3, 5 hold and the analysis ensemble $\{\mathbf{x}_{t,j}^a\}_{j=1}^n$ is generated independently from the distribution of $\mathbf{x}_t | \mathbf{y}_{1:t}$ with mean \mathbf{x}_t^a and covariance Σ_t^a at time t . If \mathcal{M}_t is approximated by $\hat{\mathcal{M}}_t$, by repeatedly performing the*

ensemble forecast-analysis process h times, at time $t + h$, the forecast and analysis states of the EnKF satisfy

$$\begin{aligned}
& p^{-1} \mathbb{E} \{ \| \hat{\mathbf{x}}_{t+h}^f - \mathbf{x}_{t+h}^f \|^2 | \mathbf{y}_{1:t+h-1} \} \\
&= O \left(n^{-1} + p^{-1} \| \mu_{\xi_{t+h}} \|^2 + p^{-1} L_{t,h}^2 (C_{t,h-1}^D)^2 \max_{t < k \leq t+h-1} \{ \Delta_{\check{\mathbf{K}}_k} \| \mathbf{y}_k - \mathbf{H}_k \mathbf{x}_k^f - \mathbf{H}_k \mu_{\xi_k} \|^2 \} \right), \\
& p^{-1} \mathbb{E} \{ \| \hat{\mathbf{x}}_{t+h}^a - \mathbf{x}_{t+h}^a \|^2 | \mathbf{y}_{1:t+h} \} \\
&= O \left(n^{-1} + p^{-1} \| (\mathbf{I} - \mathbf{K}_{t+h} \mathbf{H}_{t+h}) \mu_{\xi_{t+h}} \|^2 + p^{-1} \| \Xi_{\xi_{t+h}} \|^2 \| \mathbf{y}_{t+h} - \mathbf{H}_{t+h} \mathbf{x}_{t+h}^f \|^2 \right. \\
&\quad \left. + p^{-1} (C_{t,h}^D)^2 \max_{t < k \leq t+h} \{ \Delta_{\check{\mathbf{K}}_k} \| \mathbf{y}_k - \mathbf{H}_k \mathbf{x}_k^f - \mathbf{H}_k \mu_{\xi_k} \|^2 \} \right).
\end{aligned}$$

Compared with the result in Theorem 3.2 under the correct model, there are extra terms related to $D_{t,h} = O(\| \mathbf{I} - \mathbf{K}_k \mathbf{H}_k \| + \| \Xi_{\xi_k} \| \| \mathbf{H}_k \|)$, $\| \mu_{\xi_{t+h}} \|$ and $\| \Xi_{\xi_{t+h}} \|$ resulting from the accumulation of the approximation error of the model operator \mathcal{M}_t for the h -step assimilation MSE in Theorem 4.2. Compared with the one-step assimilation MSE in Theorem 4.1 under the imperfect models, the error term related to the approximation error of \mathcal{M}_t is inflated by $(C_{t,h}^D)^2$. The h -step assimilation MSE for the imperfect models under the fixed and high dimensions are, respectively,

$$\begin{aligned}
& \mathbb{E} \{ \| \hat{\mathbf{x}}_{t+h}^a - \mathbf{x}_{t+h}^a \|^2 | \mathbf{y}_{1:t+h} \} \asymp \max \{ (1 + (C_{t,h}^D)^2) n^{-1}, \| \mu_{\xi_{t+h}} \|^2, \| \Xi_{\xi_{t+h}} \|^2 \}, \\
& p^{-1} \mathbb{E} \{ \| \hat{\mathbf{x}}_{t+h}^a - \mathbf{x}_{t+h}^a \|^2 | \mathbf{y}_{1:t+h} \} \asymp \max \{ n^{-1}, p^{-1} \| \mu_{\xi_{t+h}} \|^2, p^{-1} q \| \Xi_{\xi_{t+h}} \|^2, (C_{t,h}^D)^2 p^{-1} q \Delta_{\check{\mathbf{K}}_k} \}.
\end{aligned} \tag{4.7}$$

Specifically, for the high dimensional case, the MSEs of the EnKF analysis state $\hat{\mathbf{x}}_{t+h}^a$ to the Kalman Filter \mathbf{x}_{t+h}^a for the h -step assimilation using the banding or mid-banding, tapering and thresholding estimates of Σ_t^f can be obtained by replacing $\Delta_{\check{\mathbf{K}}_k}$ in equation (4.7) with the specific convergence rates $(n^{-1} \log p)^{\alpha/(\alpha+1)}$, $n^{-2\alpha/(2\alpha+1)} + n^{-1} \log p$ and $c_0^2(p)(n^{-1} \log p)^{(1-\gamma)}$, respectively, according to (3.1). For the h -step assimilation, the approximation error of the model operator \mathcal{M}_t has a stronger influence on the MSE of the

data assimilation of the EnKF resulting from the accumulation of the approximation error. This highlights that a good approximation of the model operator is significant to data assimilation.

In summary, the approximation error associated with the model operator \mathcal{M}_t significantly affects the MSE in the assimilation process of the EnKF, particularly in scenarios involving multiple-step ahead data assimilation. Thus, an iterative HD-EnKF algorithm is introduced in S.1.2 of the SM to account for the model approximation error to some extent since most geophysical models are imperfect in practice, of which the main idea is to substitute $\hat{\mathbf{x}}_t^f$ in the original forecast sample covariance matrix by the analysis state $\hat{\mathbf{x}}_t^a$ in the iteration.

5 Simulation Studies

This section reports results of simulation studies performed on two popular geophysical models, the Lorenz-96 and the Shallow Water Equation models, to demonstrate the proposed HD-EnKF algorithms. These two models are often used for testing new approaches in atmospheric sciences for data assimilation and the spatial-temporal forecasts. The proposed HD-EnKFs are compared with the standard EnKF and the inflation method (Liang et al., 2012) under both the correct and imperfect models. Details of the proposed HD-EnKF algorithms are given in Section S.1 of the SM, including the consistent HD-EnKF update in S.1.1 and the iterative HD-EnKF update algorithms in S.1.2, which are based on the consistent estimators of the forecast error covariance matrix Σ_t^f by the banding, mid-banding, tapering and thresholding estimators. The iterative HD-EnKF algorithm in S.1.2 of the SM is to account for the model approximation error in the imperfect models.

5.1 Lorenz-96 model

Lorenz-96 model (L96; [Lorenz, 1996](#)) is a continuous in time but discrete in space model for modeling spatially extended chaotic systems in the atmosphere. It is a nonlinear model for continuous evolution of atmospheric variables such as temperature or vorticity at p locations on a latitude circle defined by the ordinary differential equation, for $j = 1, \dots, p$,

$$d\mathbf{x}_t^{(j)}/dt = (\mathbf{x}_t^{(j+1)} - \mathbf{x}_t^{(j-2)})\mathbf{x}_t^{(j-1)} - \mathbf{x}_t^{(j)} + F \triangleq f_j(\mathbf{x}_t, t), \quad (5.1)$$

with $\mathbf{x}_t^{(-1)} = \mathbf{x}_t^{(p-1)}$, $\mathbf{x}_t^{(0)} = \mathbf{x}_t^{(p)}$ and $\mathbf{x}_t^{(p+1)} = \mathbf{x}_t^{(1)}$, where $\mathbf{x}_t^{(j)}$ denotes the j^{th} dimension of the state variable \mathbf{x}_t , $(\mathbf{x}_t^{(j+1)} - \mathbf{x}_t^{(j-2)})\mathbf{x}_t^{(j-1)}$ is the nonlinear term, $-\mathbf{x}_t^{(j)}$ is the damping term and F is a forcing term.

L96 can be solved approximately via the fourth-order Runge-Kutta time integration scheme (RK4; [Butcher, 2016](#)), which approximates the model as $\mathcal{M}_{t+1}(\mathbf{x}_t) = \mathbf{x}_t + h(k_1 + 2k_2 + 2k_3 + k_4)/6$, where $k_1 = \mathbf{f}(\mathbf{x}_t, t)$, $k_2 = \mathbf{f}(\mathbf{x}_t + hk_1/2, t + h/2)$, $k_3 = \mathbf{f}(\mathbf{x}_t + hk_2/2, t + h/2)$, $k_4 = \mathbf{f}(\mathbf{x}_t + hk_3, t + h)$ and $\mathbf{f} = (f_1, f_2, \dots, f_p)^T$. An approximation to the true state was simulated by (i) implementing the RK4 method with a finer time step, say $h = 0.05$; and (ii) adding a random noise at each time step so that $\mathbf{x}_{t+1} = \mathcal{M}_{t+1}(\mathbf{x}_t) + \mathbf{w}_{t+1}$. In our experiment, $\mathbf{w}_t \sim N(0, \sigma_0 \mathbf{I}_p)$ and σ_0 were set as 0.1, 0.25 and 0.5, respectively. We experimented $p = 40$ and 100, under which the system behaves chaotically, since the L96 model behaves like chaos for $p \geq 7$ ([Bedrossian et al., 2022](#)). The true forcing was $F = 8$. We also considered the misspecified model setting by making $F = 6, 7, 9, 10$ in the assimilation processes, corresponding to the imperfect models in Section 4. The initial state was $x_1^{(j)} = F$ for $j \neq 20$ and $x_1^{(20)} = F + 0.001$, and the initial forecast ensemble was generated by $\mathbf{x}_{1,j}^f = \mathbf{x}_1 + N_p(0, 0.1 \mathbf{I}_p)$ for $j = 1, \dots, n$.

The observations \mathbf{y}_t were made at q randomly selected components of the state vector \mathbf{x}_t with $q = 30, 40$ and 100 while $p = 40$ and 100, respectively, followed by adding

observation errors $\boldsymbol{\varepsilon}_t \stackrel{IID}{\sim} N_q(0, \mathbf{R}_t)$ to the true states. The (i, j) -element of \mathbf{R}_t was $R_{ij} = 0.5^{\min\{|i-j|, q-|i-j|\}}$, which prescribes spatially correlated observation errors. The observation operator \mathbf{H}_t was a $q \times p$ matrix with the (j, i) element being 1 if the j -th component of \mathbf{y}_t was the observed i -th dimension of the state \mathbf{x}_t . We simulated observations every 4 time steps for a total of 2000 steps and reported the results for the last 1000 steps to allow the system to settle down. The ensemble size n was 20, 30, 60 and 90. All the experiments were repeated 500 times.

We considered the HD-EnKF schemes using the banding, mid-banding, tapering and thresholding covariance estimators, which were compared with the standard EnKF that utilizes the sample covariance and the inflation methods (Liang et al., 2012). The performances of these methods were evaluated by the root-mean-square error (RMSE) of the analysis state $\hat{\mathbf{x}}_t^a$ to (i) the underlying analysis state \mathbf{x}_t^a by the Kalman Filter utilizing the true covariances and (ii) the true state \mathbf{x}_t . To gain accurate estimations of $\boldsymbol{\Sigma}_t^f$ for the oracle analysis \mathbf{x}_t^a , we used the standard EnKF with a very large ensemble size 1000 (relative to p in the simulation), and used the sample covariance to replace $\boldsymbol{\Sigma}_t^f$ in the Kalman Filter update formula to obtain \mathbf{x}_t^a .

Figure 2 displays the average RMSEs to the oracle analysis state of the five assimilation methods, namely the standard EnKF, the inflation method and the three HD-EnKFs equipped with the banding and tapering (both respect the circular bandable structures), and the thresholding estimators, under different forcing F at moderate dimension $p = 40$ and high dimension $p = 100$ with different σ_0 and n . It shows that the HD-EnKF with the three high dimensional covariance estimators had much smaller RMSEs than the standard EnKF and the inflation methods at both the correct ($F = 8$) and misspecified ($F \neq 8$) models. Even when F deviated more from the true value 8, the HD-EnKFs still achieved

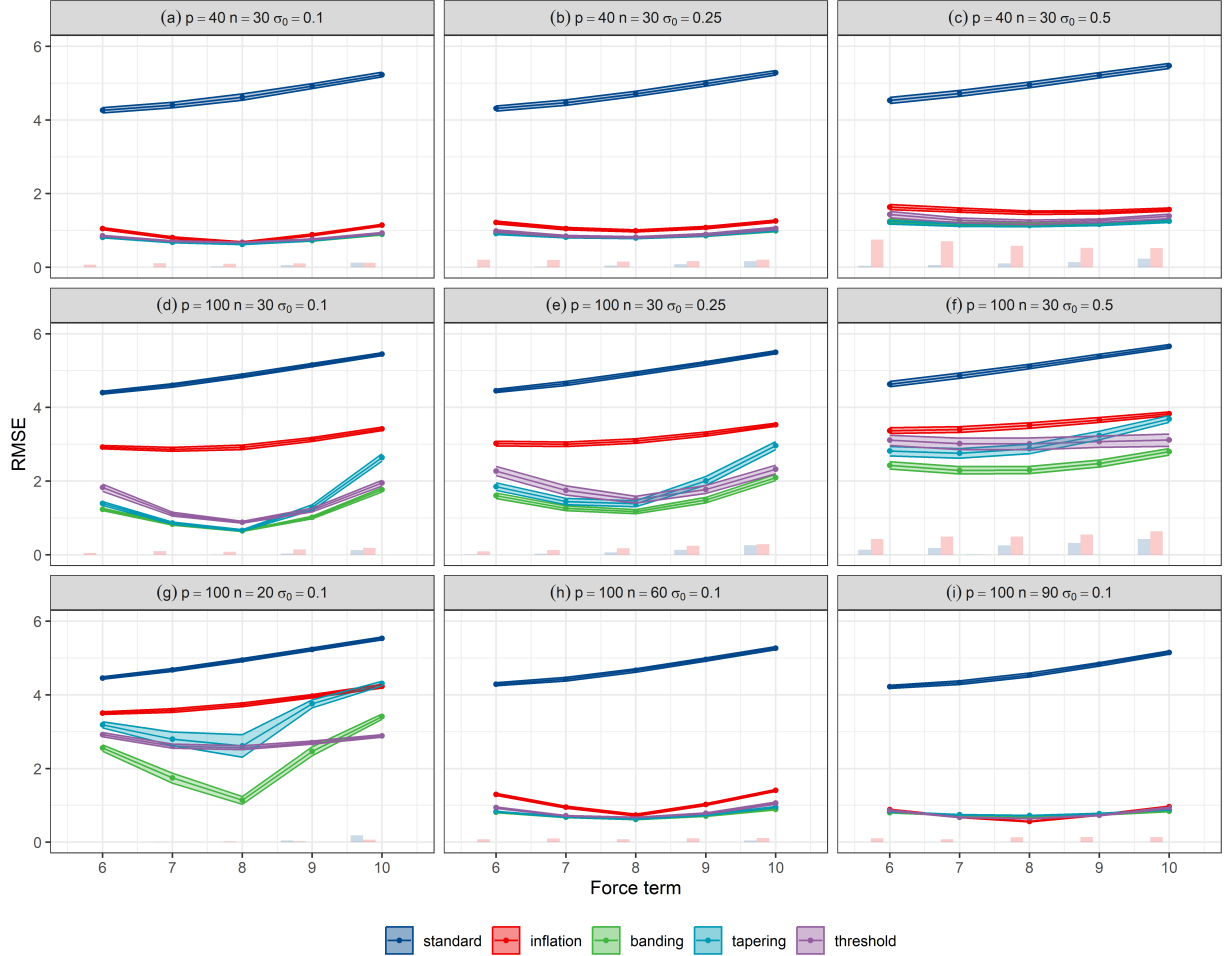


Figure 2: Average RMSEs to the oracle analysis state and their 25 – 75% quantile bands (color bands) as a function of forcing F used in \mathcal{M}_t (true value is 8) by the standard EnKF (blue), the modified EnKF methods: the inflation (red), banding (green), tapering (cyan) and thresholding (purple) for $p = q = 40$ and 100 , $n = 20, 30, 60, 90$, $\sigma_0 = 0.1, 0.25$ and 0.5 , respectively. The light-colored bars in the lower part of each panel denote the divergence rates of the assimilation schemes.

analysis states much closer to the oracle than the inflation method, although both strains of methods showed increased RMSEs with respect to $|F - 8|$. The standard EnKF with the sample covariance estimator had much larger assimilation errors in all cases.

Comparing Figure 2's panels (d)-(f) with panels (a)-(c), the advantages of the proposed HD-EnKFs over the inflation method were more apparent for the higher dimension $p = 100$. The analysis RMSEs of the HD-EnKFs kept at a lower level especially when the force F was equal or close to the true value ($F = 8$), while the analysis RMSE of the inflation method

ranked behind but better than the standard EnKF. This means that the HD-EnKFs are quite attractive as the geophysical models in earth science are of ultra high dimension. The figure also displays the percentages of divergence of the five methods. The inflation method endured quite high divergences which increased substantially with the model error (e.g. reached 50% when $\sigma = 0.5$), even higher than the standard EnKF. In contrast, the three HD-EnKF methods had quite low divergence rates for all cases.

Panels (d), (g)-(f) of Figure 2 demonstrate the influence of the ensemble size on the analysis RMSEs. Although the analysis RMSEs of the inflation and the HD-EnKF methods all became smaller with the increase of the ensemble size n , the proposed HD-EnKFs outperformed the inflation method, especially when the ensemble size n was small (panels (d) and (g) with $n = 20$). This suggests that the proposed methods could provide more accurate analysis states when the ensemble size was not big enough. Ensemble size is a significant restriction for the large geophysical models as they are extremely costly to run.

Table 1 displays the analysis RMSEs of different methods and their divergence rates under sparser observations $q = 30$ while $p = 40$, which illustrates the influence of the sparsity in the observations on the assimilation accuracy. Although the analysis RMSEs of different assimilation methods were slightly higher than those under more observations $p = q = 40$, the RMSEs of the HD-EnKF methods were smaller than those of the other methods for imperfect models ($F \neq 8$) and were comparable to the inflation method for the correct model ($F = 8$). However, it is noted that the inflation method had a higher divergence rate which reached 63% even under the correct model ($F = 8$) while the proposed methods had low divergence rates, showing their robustness to the sparsity of the observations.

Table 1: Average RMSEs to the oracle analysis state and true state of the five EnKF schemes and their divergence rates (in parentheses) for Lorenz-96 model with $p = 40$, $q = 30$, $n = 30$, $\sigma_0 = 0.1$, and $F = 8$ for the correct and other F values for misspecified models.

	method	F=6	F=7	F=8	F=9	F=10
oracle	standard	4.26 (0.01)	4.43 (0.06)	4.69 (0.15)	5.05 (0.29)	5.41 (0.54)
	inflation	1.32 (0.80)	0.96 (0.65)	0.77 (0.63)	1.03 (0.69)	1.38 (0.86)
	banding	1.10 (0.11)	0.90 (0.08)	0.83 (0.09)	0.99 (0.12)	1.27 (0.29)
	tapering	1.08 (0.13)	0.87 (0.07)	0.79 (0.06)	0.99 (0.13)	1.31 (0.25)
	threshold	1.12 (0.06)	0.90 (0.02)	0.84 (0.04)	1.00 (0.04)	1.35 (0.16)
true	standard	4.28 (0.01)	4.44 (0.06)	4.70 (0.15)	5.05 (0.29)	5.40 (0.54)
	inflation	1.42 (0.80)	1.04 (0.65)	0.84 (0.63)	1.11 (0.69)	1.47 (0.86)
	banding	1.23 (0.11)	1.01 (0.08)	0.93 (0.09)	1.09 (0.12)	1.37 (0.29)
	tapering	1.21 (0.13)	0.98 (0.07)	0.90 (0.06)	1.09 (0.13)	1.42 (0.25)
	threshold	1.24 (0.06)	1.00 (0.02)	0.93 (0.04)	1.09 (0.04)	1.44 (0.16)

5.2 Shallow Water Equation model

The second experiment was conducted on the Shallow Water Equation model (SWE). The SWE is a system of hyperbolic/parabolic partial differential equations governing fluid flow, which is widely used in river flow simulations, as well as in other settings where the water depth is significantly lower than the horizontal length scale of motion. The barotropic nonlinear SWE takes the following form (Lei et al., 2012), for $0 \leq z_1 \leq L, 0 \leq z_2 \leq D$,

$$\begin{aligned}
 \frac{\partial u}{\partial t} + u \frac{\partial u}{\partial z_1} + v \frac{\partial u}{\partial z_2} - fv &= -g \frac{\partial h}{\partial z_1} + k \nabla^2 u, \\
 \frac{\partial v}{\partial t} + u \frac{\partial v}{\partial z_1} + v \frac{\partial v}{\partial z_2} + fu &= -g \frac{\partial h}{\partial z_2} + k \nabla^2 v, \\
 \frac{\partial h}{\partial t} + u \frac{\partial h}{\partial z_1} + v \frac{\partial h}{\partial z_2} &= -h \left(\frac{\partial u}{\partial z_1} + \frac{\partial v}{\partial z_2} \right) + k \nabla^2 h,
 \end{aligned} \tag{5.2}$$

where the fluid velocity components u in z_1 direction and v in z_2 direction as well as the fluid depth h are the model variables, g is the gravity acceleration 9.8 m s^{-2} , f is the Coriolis parameter defined as constant 10^{-4} s^{-1} , k is the diffusion coefficient specified as

$5 \times 10^4 \text{ m}^2 \text{ s}^{-1}$, and L and D are the domain limits set as 500 km and 300 km, respectively.

The SWE was discretized with a uniform grid spacing of 10 km in the z_1 and z_2 directions and solved by the Lax-Wendroff method with a time step of 30 seconds. Thus, the SWE model had a dimension of $p' = 50 \times 31$ for each state variable u, v, h , leading to the state vector $\mathbf{x}_t = (u_t, v_t, h_t)^T$ of dimension $p = 3p' = 4650$. The initial height (depth) was given by $h(z_1, z_2) = H_0 + H_1 \tanh\left(9(D/2 - z_2)/2/D\right) + H_2 \operatorname{sech}^2\left(9(D/2 - z_2)/D\right) \sin\left(2\pi z_1/L\right)$, where H_0, H_1 and H_2 were set to be 50 m, 5.5 m and 3.325 m, respectively. The initial velocity field was derived from the initial height field with the geostrophic relation.

The SWE was simulated for 48 hours with a total of 5760 time steps at 30 second intervals after a half hour (60-steps) pre-running. The observations of u, v and h were made at $q' = 310$ grid points from 10 randomly selected rows in each direction every 3 hours, making the whole observation vector $\mathbf{y}_t = (u_t, v_t, h_t)^T$ be of dimension $q = 3q' = 930$, which means the observations were quite sparse with $q = 0.2p$. To generate the imperfect models, the diffusion coefficient k was also considered as $10^4 \text{ m}^2 \text{ s}^{-1}$ in the assimilation process. The observation error variances were $\sigma_u^2 = \sigma_v^2 = 0.5, \sigma_h^2 = 1.0$ for the three dimensions and $\mathbf{R}_t = \operatorname{diag}(\sigma_u^2 \mathbf{I}_{p'}, \sigma_v^2 \mathbf{I}_{p'}, \sigma_h^2 \mathbf{I}_{p'})$. The ensemble size n was 100, and the initial ensemble was generated by adding random noises from $\mathcal{N}_p(0, \mathbf{I}_p)$ to the initial state \mathbf{x}_1 .

Figure 3 reports the RMSEs at each assimilation time step of the five EnKF methods (the standard EnKF, inflation and three HD-EnKF) to the oracle analysis states \mathbf{x}_t^a and the true states \mathbf{x}_t under the correct ($k = 5 \times 10^4$) and the imperfect ($k = 10^4$) models while Table 2 summarizes the average analysis RMSEs over the last 24 hours (2880 steps), together with their 25% and 75% quantiles. Figure 3 shows the three proposed HD-EnKF methods outperformed the inflation and the standard EnKF methods for both the correct and imperfect models with much smaller RMSEs after the system settled down and that

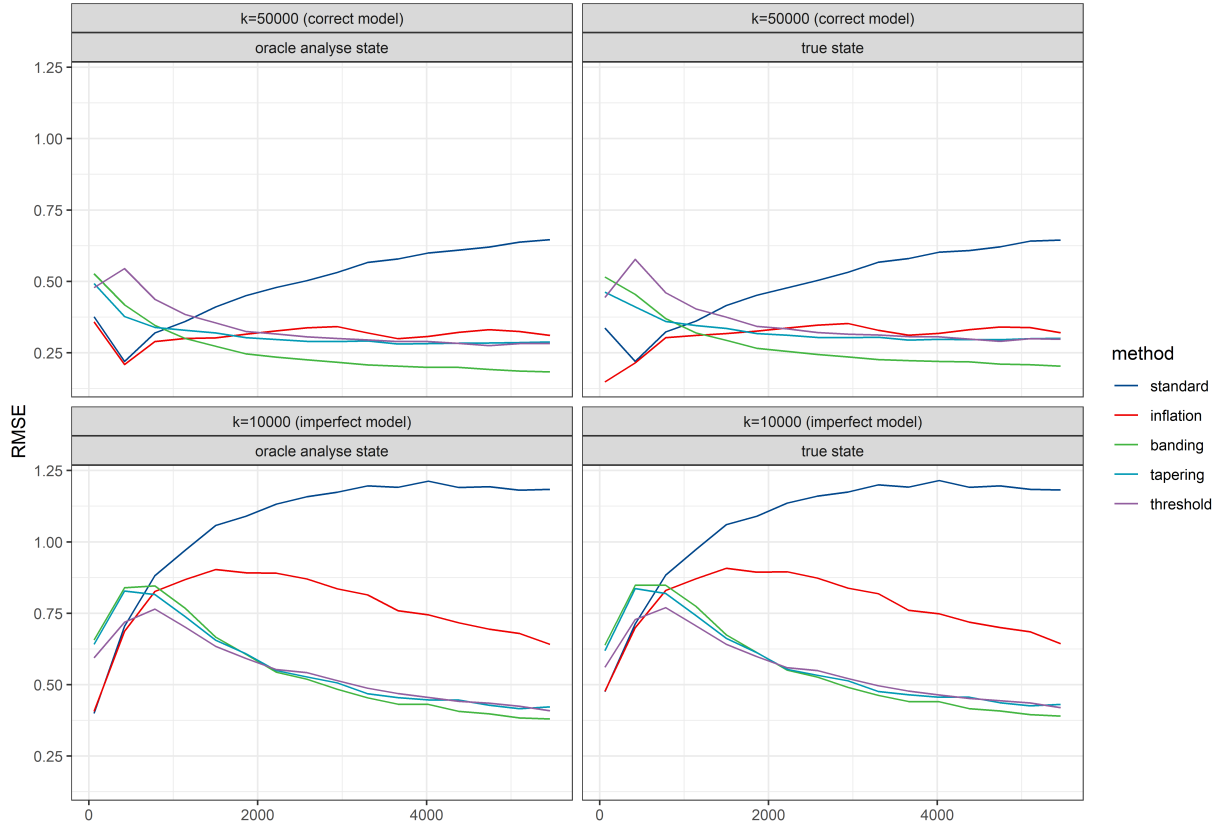


Figure 3: RMSEs to the oracle analysis state (left panels) and the true state (right panels) at each assimilation step by the standard, inflation, banding, tapering and threshold under the correct model ($k = 5 \times 10^4$) and imperfect model ($k = 10^4$) with $n = 100$, $p = 4650$ and $q = 930$ on the SWE model.

the superiority became more apparent over time, especially under the misspecified model. Specifically, the RMSEs at each assimilation time step of the three proposed HD-EnKF schemes became lower and lower over time compared to increased RMSEs for the standard EnKF for all cases and for the inflation method under true models.

It is obvious from Table 2 that the HD-EnKF methods had significantly lower RMSEs and narrower 25%-75% quantile bands with more evident superiority under imperfect models. Specifically, the proposed HD-EnKFs could reduce the RMSE by 41% compared to the inflation method, implying that the proposed methods could attain more accurate and robust assimilated results even under extremely sparse observations and high dimensional states. Thus, the proposed methods are highly appealing, especially considering the high

Table 2: Average RMSEs to the oracle analysis state and true state over the last 24 hours (2880 steps) and their 25% and 75% quantiles (in parentheses) by the five EnKF schemes for the SWE model under the correct ($k = 5 \times 10^4$) and the imperfect ($k = 10^4$) models with $n = 100$, and $p = 4650$ and $q = 930$.

method	k = 50000 (correct model)		k = 10000 (imperfect model)	
	oracle	true	oracle	true
standard	0.61 (0.45, 0.76)	0.62 (0.47, 0.78)	1.16 (1.05, 1.26)	1.18 (1.07, 1.28)
inflation	0.34 (0.27, 0.40)	0.38 (0.31, 0.44)	0.75 (0.68, 0.82)	0.77 (0.70, 0.84)
banding	0.20 (0.17, 0.22)	0.26 (0.23, 0.28)	0.42 (0.40, 0.45)	0.46 (0.43, 0.48)
tapering	0.25 (0.23, 0.28)	0.30 (0.28, 0.33)	0.44 (0.41, 0.46)	0.47 (0.44, 0.50)
threshold	0.28 (0.26, 0.30)	0.33 (0.31, 0.35)	0.44 (0.42, 0.46)	0.48 (0.46, 0.50)

dimensional geophysical models in earth science.

6 Discussion

In this paper, we propose HD-EnKF algorithms to suit the needs of high dimensional data assimilation. We take the opportunity to study the theoretical properties of the EnKF under both the fixed and the high dimensional cases for both the correct and misspecified models. The study shows that the proposed HD-EnKF can replace the widely used inflation method for data assimilation of a large dynamic system based on two considerations. One is that the established theoretical analysis on the consistency and the error bounds makes the proposed HD-EnKF methods more understandable with a theoretical guarantee; and the other is the better algorithm convergence and smaller RMSEs than the inflation method as shown in the simulation studies. The latter means that a smaller ensemble size for the EnKF can be used at a given level of accuracy which is particularly attractive as the running of the geophysical models is generally very expensive. The proposed HD-EnKF has great potential for applications in earth science where the geophysical models, the state variables

or the observations are high dimensional, such as global carbon calculation, ocean data assimilation, weather forecasting, sea ice prediction and the generation of high-resolution data sets.

SUPPLEMENTARY MATERIAL

We provide detailed steps of the proposed HD-EnKF algorithm, bandwidth selection of the mid-banding estimator, additional theoretical results and simulation results, and the details for the proofs of the theoretical results in the Supplementary.

References

Al-Ghattas, O., J. Bao, and D. Sanz-Alonso (2024). Ensemble kalman filters with resampling. *SIAM/ASA Journal on Uncertainty Quantification* 12(2), 411–441.

Al-Ghattas, O., J. Chen, D. Sanz-Alonso, and N. Waniorek (2025). Covariance operator estimation: Sparsity, lengthscale, and ensemble kalman filters. *Bernoulli* 31(3), 2377–2402.

Al-Ghattas, O. and D. Sanz-Alonso (2024). Non-asymptotic analysis of ensemble kalman updates: Effective dimension and localization. *Information and Inference: A Journal of the IMA* 13(1), iaad043.

Anderson, J. L. and S. L. Anderson (1999). A Monte Carlo implementation of the nonlinear filtering problem to produce ensemble assimilations and forecasts. *Monthly Weather Review* 127(12), 2741–2758.

Bai, Z. D. and Y. Q. Yin (1993). Limit of the smallest eigenvalue of a large dimensional sample covariance matrix. *The Annals of Probability* 21(3), 1275 – 1294.

Bedrossian, J., A. Blumenthal, and S. Punshon-Smith (2022). A regularity method for lower bounds on the Lyapunov exponent for stochastic differential equations. *Inventiones mathematicae* 227(2), 429–516.

Bickel, P. J. and E. Levina (2008a). Covariance regularization by thresholding. *The Annals of Statistics* 36(6), 2577–2604.

Bickel, P. J. and E. Levina (2008b). Regularized estimation of large covariance matrices. *The Annals of Statistics* 36(1), 199–227.

Bouttier, F. and P. Courtier (1999). Data assimilation concepts and methods march 1999.

Butcher, J. C. (2016). *Numerical Methods for Ordinary Differential Equations* (First ed.). Wiley.

Cai, T. T., C.-H. Zhang, and H. H. Zhou (2010). Optimal rates of convergence for covariance matrix estimation. *The Annals of Statistics* 38(4), 2118–2144.

Constantinescu, E. M., A. Sandu, T. Chai, and G. R. Carmichael (2007). Ensemble-based chemical data assimilation. I: General approach. *Quarterly Journal of the Royal Meteorological Society* 133(626), 1229–1243.

Courtier, P., E. Andersson, W. Heckley, D. Vasiljevic, M. Hamrud, A. Hollingsworth, F. Rabier, M. Fisher, and J. Pailleux (1998). The ECMWF implementation of three-dimensional variational assimilation (3D-Var). I: Formulation. *Quarterly Journal of the Royal Meteorological Society* 124(550), 1783–1807.

Evensen, G. (1994). Sequential data assimilation with a nonlinear quasi-geostrophic model using Monte Carlo methods to forecast error statistics. *Journal of Geophysical Research* 99(C5), 10143.

Evensen, G., F. C. Vossepoel, and P. J. van Leeuwen (2022). Data Assimilation Fundamentals: A Unified Formulation of the State and Parameter Estimation Problem. Cham: Springer International Publishing.

Furrer, R. and T. Bengtsson (2007). Estimation of high-dimensional prior and posterior covariance matrices in Kalman filter variants. Journal of Multivariate Analysis 98(2), 227–255.

Furrer, R., M. G. Genton, and D. Nychka (2006). Covariance tapering for interpolation of large spatial datasets. Journal of Computational and Graphical Statistics 15(3), 502–523.

Guinehut, S., A.-L. Dhomps, G. Larnicol, and P.-Y. Le Traon (2012). High resolution 3-D temperature and salinity fields derived from in situ and satellite observations. Ocean Science 8(5), 845–857.

Houtekamer, P. L. and H. L. Mitchell (1998). Data assimilation using an Ensemble Kalman Filter technique. Monthly Weather Review 126(3), 796–811.

Julier, S. J. and J. K. Uhlmann (1997). New extension of the kalman filter to nonlinear systems. In Signal processing, sensor fusion, and target recognition VI, Volume 3068, pp. 182–193.

Kalman, R. E. (1960). A new approach to linear filtering and prediction problems. Journal of Basic Engineering 82(1), 35–45.

Katzfuss, M., J. R. Stroud, and C. K. Wikle (2020). Ensemble kalman methods for high-dimensional hierarchical dynamic space-time models. Journal of the American Statistical Association 115(530), 866–885.

Kwiatkowski, E. and J. Mandel (2015). Convergence of the square root ensemble kalman filter in the large ensemble limit. *SIAM/ASA Journal on Uncertainty Quantification* 3(1), 1–17.

Le Gland, F., V. Monbet, and V.-D. Tran (2009). *Large Sample Asymptotics for the Ensemble Kalman Filter*. Ph. D. thesis, INRIA, Rennes, France.

Lei, L., D. R. Stauffer, and A. Deng (2012). A hybrid nudging-ensemble kalman filter approach to data assimilation. part ii: application in a shallow-water model. *Tellus A: Dynamic Meteorology and Oceanography* 64(1), 18485.

Lellouche, J. M., O. Le Galloudec, M. Dréville, C. Régnier, E. Greiner, G. Garric, N. Ferry, C. Desportes, C. E. Testut, C. Bricaud, R. Bourdallé-Badie, B. Tranchant, M. Benkiran, Y. Drillet, A. Daudin, and C. De Nicola (2013). Evaluation of global monitoring and forecasting systems at mercator océan. *Ocean Science* 9(1), 57–81.

Liang, X., X. Zheng, S. Zhang, G. Wu, Y. Dai, and Y. Li (2012). Maximum likelihood estimation of inflation factors on error covariance matrices for ensemble Kalman filter assimilation: MLE of inflation factors on error covariance matrices for EnKF. *Quarterly Journal of the Royal Meteorological Society* 138(662), 263–273.

Lorenc, A. C. (2003). The potential of the ensemble kalman filter for nwp—a comparison with 4d-var. *Quarterly Journal of the Royal Meteorological Society* 129(595), 3183–3203.

Lorenz, E. N. (1963). Deterministic nonperiodic flow. *Journal of Atmospheric Sciences* 20(2), 130 – 141.

Lorenz, E. N. (1996). Predictability: A problem partly solved. In *Proc. Seminar on predictability*, Volume 1, pp. 1–18.

Pailleux, J. (1990). A global variational assimilation scheme and its application for using tovs radiances. In Proc. WMO International Symposium on Assimilation of Observations in Meteorology and Oceanography, pp. 325–328.

Qiu, Y. and S. X. Chen (2015). Bandwidth selection for high-dimensional covariance matrix estimation. Journal of the American Statistical Association 110(511), 1160–1174.

Stroud, J. R., M. L. Stein, B. M. Lesht, D. J. Schwab, and D. Beletsky (2010). An Ensemble Kalman Filter and smoother for satellite data assimilation. Journal of the American Statistical Association 105(491), 978–990.

Thepaut, J.-N. and P. Courtier (1991). Four-dimensional variational data assimilation using the adjoint of a multilevel primitive-equation model. Quarterly Journal of the Royal Meteorological Society 117(502), 1225–1254.

Tong, X. T. (2018). Performance analysis of local ensemble kalman filter. Journal of Nonlinear Science 28(4), 1397–1442.

Wang, X. and C. H. Bishop (2003). A comparison of breeding and ensemble transform Kalman filter ensemble forecast schemes. Journal of the Atmospheric Sciences 60(9), 1140–1158.